International Journal of Solids and Structures 45 (2008) 5765–5787

Contents lists available at ScienceDirect

International Journal of Solids and Structures

journal homepage: www.elsevier.com/locate/ijsolstr

An anisotropic fibre-network model for mechano-sorptive creep in paper

Jessica Strömbro, Peter Gudmundson *

KTH Solid Mechanics, Royal Institute of Technology, Osquars backe 1, SE-100 44 Stockholm, Sweden

ARTICLE INFO

Article history:
Received 5 March 2008
Received in revised form 23 May 2008
Available online 24 June 2008

Keywords:
Mechano-sorptive creep
Accelerated creep
Paper
Modelling
Moisture changes
Humidity change
Sorption
Fibres
Creep
Network model
Fibre network
Mathematical model
Fibre bonding
Tension
Compression
Anisotropy

ABSTRACT

In this paper a simplified network model for mechano-sorptive creep is presented, which is a further development of an earlier paper [Strömbro, J., Gudmundson, P., 2008. Mechano-sorptive creep under compressive loading – a micromechanical model. International Journal of Solids and Structures 45 (9), 2420–2450.]. It is assumed that the anisotropic hygro-expansion of the fibres leads to large stresses at the fibre bonds when the moisture content changes. The resulting stress state will accelerate creep if the fibre material obeys a constitutive law that is non-linear. Fibre kinks are included in order to capture experimental observations of larger mechano-sorptive effects in compression than in tension. Moisture dependent material parameters and anisotropy in the fibre distribution have been introduced. Theoretical predictions based on the model are compared to experimental results for an anisotropic paper both under tensile and compressive loading at varying moisture content and it is found that the important features in the experiments are captured by the model. Different kinds of drying conditions have also been examined.

1. Introduction

Paper and corrugated board packages are often loaded for long times, and therefore creep, i.e. time dependent deformation, is an important factor in package design. Boxes are in addition exposed to environmental cycling during their lifetime, for example caused by weather and seasonal changes, but also as they are moved between different storages. Paper is sensitive to moisture and creep of paper is affected by humidity conditions. The creep rate generally increases with increasing humidity, i.e. increasing moisture content in the paper (Brezinski, 1956). High humidity is however not the worst possible environment as creep is also accelerated by varying humidity. Creep during cycling between low and high humidity is likely to exceed the creep at constant humidity even at the highest level, a phenomenon known as mechano-sorptive creep or accelerated creep (Byrd, 1972a,b; Söremark and Fellers, 1993; Söremark et al., 1993; Haslach, 1994; Habeger and Coffin, 2000). Mechano-sorptive creep in paper has been known since 1972 (Byrd, 1972a,b), but was discovered first in wool (Mackay and Downes, 1959; Nordon, 1962) and wood (Armstrong and Kingston, 1960; Armstrong and Christensen, 1961) in the late 1950s and early 1960s. A similar behaviour has also been found in concrete (Pickett, 1942) and in the 1990s mechano-sorptive creep was found in some synthetic fibres (Wang et al., 1990, 1992, 1993).

* Corresponding author. Tel.: +46 8 790 75 48; fax: +46 8 411 24 18.
E-mail address: peter@hallf.kth.se (P. Gudmundson).

0020-7683/$ - see front matter © 2008 Elsevier Ltd. All rights reserved.
doi:10.1016/j.ijsolstr.2008.06.010

Even though mechano-sorptive creep was discovered several decades ago, there is still no generally accepted model for the phenomenon. Several models and hypotheses about the physical mechanisms have been proposed. It has for example been suggested that moisture content changes cause breaking of hydrogen bonds (Gibson, 1965) or that it generates free volume in the material (Padanyi, 1991, 1993), both explanations would lead to an increase in creep compliance. The mechano-sorptive effect has also been explained by dislocations, which are created and affected by stresses caused by moisture content changes. Compressive loading would lead to an increased number of dislocations and more dislocations lead to a higher hygroexpansion and lower stiffness (Hoffmeyer and Davidson, 1989; Hoffmeyer, 1993; Söremark and Fellers, 1993). A model combining the above mentioned mechanisms, has also been proposed (Haslach, 1994). By experiments using IR-spectra it has been indicated that additional creep mechanisms on a molecular level are activated during moisture cycling compared to constant moisture (Olsson and Salmén, 2001). Phenomenological models that do not take actual micro-mechanisms into account have also been presented (Ranta-Maunus, 1975; Mårtensson, 1994; Urbanik, 1995).

In some recent investigations (Habeger and Coffin, 2000; Alfthan et al., 2002; Alfthan, 2003, 2004; Alfthan and Gudmundson, 2005; Strömbro and Gudmundson, 2008) it has been suggested that mechano-sorptive creep in paper is an effect of non-linear creep of the individual fibres in combination with large transient stresses created during moisture content changes which give rise to redistribution of stresses. The stresses are created by inhomogeneous hygroexpansion in the material. The inhomogeneous hygroexpansion can be caused by material heterogeneities, mainly that the fibre swelling and shrinkage due to moisture content changes are much larger transverse to the fibre axis in comparison to the axial direction of the fibres (Gallay, 1973). When moisture is changed, the fibres will expand (or shrink). At the bonds, the expansion is restricted by the crossing fibres because of the anisotropic hygroexpansive properties. Instead large stresses are created. In resemblance with the material heterogeneities, inhomogeneous hygroexpansive strains can also be caused by moisture gradients, which introduce similar internal stresses because of the restriction by the surrounding material. The internal stresses will be added to the stress state caused by external mechanical loads (van den Akker, 1962). If the creep depends non-linearly on the stress this stress redistribution gives rise to an increased creep rate. The stress state produced by the change in moisture is transient and after a while a new change in moisture content is required to create a new redistribution of stresses and to further accelerate the creep. The advantage of this kind of model compared to others is that accelerated creep turns out to be a natural consequence of regular creep, and no special mechanism must be introduced to explain mechano-sorptive creep. It has been shown that accelerated creep is obtained by models based on this mechanism (Habeger and Coffin, 2000; Alfthan et al., 2002; Alfthan, 2003, 2004; Alfthan and Gudmundson, 2005; Strömbro and Gudmundson, 2008).

Bonds are believed to be necessary for mechano-sorptive creep, but how they affect the mechano-sorptive creep has not been examined to any great. Recently Demaio and Patterson with co-workers have examined how the bonding influences the creep and mechano-sorptive creep behaviour in paper (DeMaio et al., 2006; DeMaio and Patterson, 2006, 2007, 2008). They have performed experiments on paper with different bond strengths between the fibres. The results showed that, as long as there is a sufficient bonding between the fibres, additional increase of the bonding strength does not influence constant humidity creep or mechano-sorptive creep. They also found that bonding has no additional effect on mechano-sorptive creep behaviour beyond the effect on the constant humidity creep behaviour. They concluded that their experimental results support the argument that the mechanisms behind constant humidity creep and accelerated creep are the same (DeMaio and Patterson, 2008).

There are many experimental observations that indicate a different behaviour in compression in comparison to tension (Armstrong and Kingston, 1962; Byrd, 1972a,b; Söremark and Fellers, 1993; Söremark et al., 1993). It has been shown that the mechano-sorptive effects are larger in compression than in tension. In addition, the modulus of elasticity of paper is altered by mechano-sorptive creep, it decreases under mechano-sorptive creep in compression and it increases in tension. In Fig. 1 mechano-sorptive creep is shown from experiments on kraft paper produced at STFI-Packforsk which was dried under restraint and had a grammage of 100 g/m^2 and a thickness of 0.121 mm, in both tensile and compressive loading. It can be observed that the paper creeps faster in compression, which leads to more deformation at a given time and stress level.

Since compression and bending are the most important load cases in packages, the additional accelerated creep in compression compared to tension is important to examine. A model describing this difference should also be able to capture the mechano-sorptive creep behaviour in bending, since bending induces compression and tensile strains in the paper (Söremark and Fellers, 1993; Söremark et al., 1993).

The differences between tensile and compressive behaviour are probably an effect of the geometrical fibre properties, e.g. fibre curl and kinks. As pointed out earlier in this section, the moisture expansion in the transverse direction of a fibre is much larger than that in the longitudinal direction. If an initially curved fibre is considered, an increase in moisture content will then decrease the curvature, and vice versa. The load also affects the curvature; a tensile load will decrease the curvature, while the curvature will increase with increasing compressive load. As a consequence the stiffness will decrease with increased compressive loading, and vice versa, since the fibre compliance increases with the curvature. A network model that included the effects of fibre geometry such as curvature has been presented in an earlier work (Strömbro and Gudmundson, 2008). That model was able to capture mechano-sorptive creep both under tension and compression and the differences between these two load cases.

In the present work, the above mentioned network model is further developed. Anisotropy in the fibre distribution and variations in the fibre kink are introduced in the model as well as moisture dependent material parameters. First the micromechanical model with geometrical fibre effects included is presented. Then the experimental work is described. In order to apply the model a number of material parameters is determined. Theoretical predictions based on the developed model can

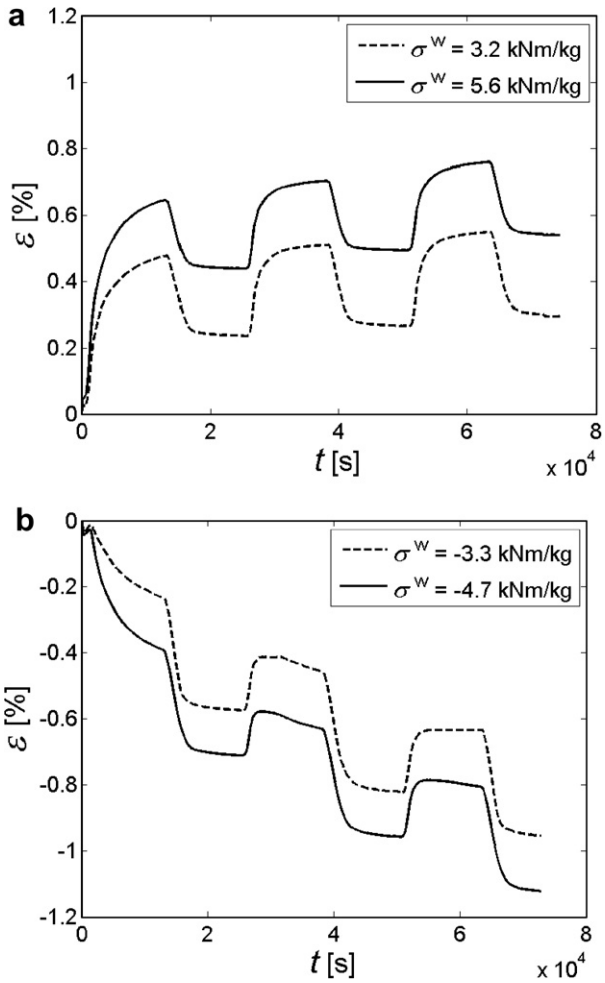

Fig. 1. Results from mechano-sorptive creep experiments (done by STFI-Packforsk) on kraft paper which was dried under restraint and had a grammage of 100 g/m^2 and a thickness of 0.121 mm in tension (a) and compression (b) at different specific stress levels. The relative humidity was cycled between 50% RH and 90% RH.

then be compared to experimental results for paper both under tensile and compressive loading at varying moisture content. Different types of drying conditions are also examined and discussed. Finally, conclusions are drawn.

2. Micromechanical model

The network model presented here is a further development of the model described in an earlier work (Strömbro and Gudmundson, 2008). The macroscopic paper properties were derived by a homogenization procedure. The model is based on the work by Alfthan (2003), but with a more advanced fibre model, including kinked fibre segments to capture experimental observations for paper loaded in both tension and compression. Alfthan's network model is based on the same idea as the network model by Cox from 1952, which was a first attempt to model the influence of fibres on sheet properties (Cox, 1952). Cox's model only considered elastic behaviour while Alfthan's model added hygroexpansion, creep, and the influence of bonds. The model has now been further developed, anisotropy in the fibre distribution is introduced and also moisture dependent material parameters. A description of the model is given below, however a more detailed description of some parts of the model can be found in the earlier work (Strömbro and Gudmundson, 2008).

In a fibre network, each fibre is bonded to many other fibres and hence each fibre consists of free and bonded segments, sections A and B, see Figs. 2 and 3. The free fibre segments between the fibre bonds are modelled using the fibre model described in the paper by Strömbro and Gudmundson (2008). The model does not include any effects of the finite length of fibres in real paper, i.e. the fibres are assumed to be long, well-bonded fibres. A fibre consists of fibre segments which in its turn are divided into a free fibre segment and a bonded fibre segment. The length of the free fibre segment is denoted L_f and the total length of the segment is denoted L (see Fig. 3). If the strain of the free segments of a fibre is ε_A and the strain

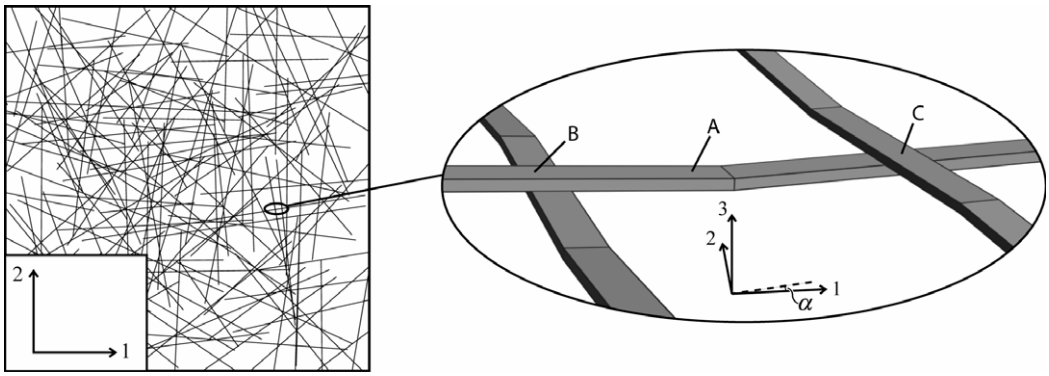

Fig. 2. The fibre-network where each fibre is bonded to many other fibres. For each fibre segment the fibre model is used. A, B and C denotes the different fibre parts.

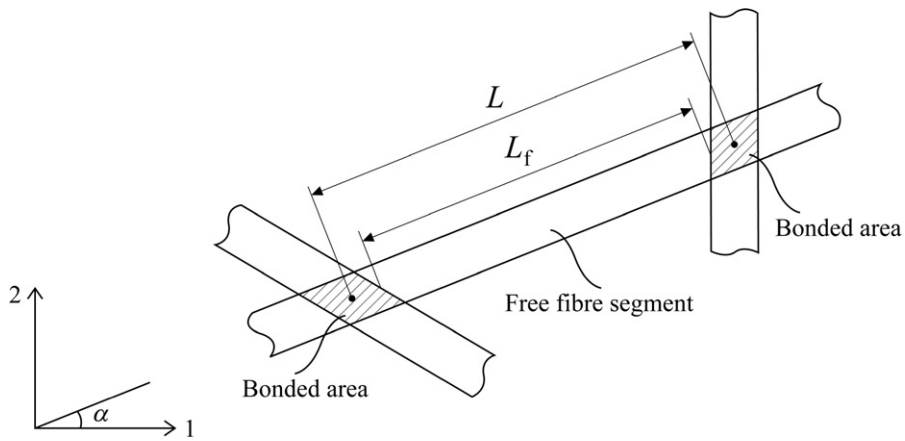

Fig. 3. The geometry of a fibre segment. The direction of the fibre is defined by the angle α measured from the 1-axis of the coordinate system.

of the bonded length is ε_B, then the average strain of the fibre segment, which also corresponds to the average strain in a fibre, will be

$$\varepsilon = \lambda\varepsilon_A + (1-\lambda)\varepsilon_B, \tag{1}$$

where $\lambda = L_f/L$. It is assumed that the average normal strain ε of each fibre is prescribed by the macroscopic strains $\bar{\varepsilon}_{11}, \bar{\varepsilon}_{22}$ and $\bar{\varepsilon}_{12}$, where 1 and 2 denotes the coordinate direction in the plane of the paper and the bar indicates a macroscopic quantity. The average strain of a fibre ε is then given by

$$\varepsilon = \bar{\varepsilon}_{11}\cos^2\alpha + \bar{\varepsilon}_{22}\sin^2\alpha + 2\bar{\varepsilon}_{12}\cos\alpha\sin\alpha, \tag{2}$$

where α is the angle of the fibre with respect to the 1-axis (see Fig. 3).

The bonded sections of a fibre are assumed to behave as a composite of the fibre itself and the crossing fibre. Since a perfect bonding is assumed, the transverse strain ε_C of the crossing fibres in the bonded area, section C in Fig. 2, will be the same as the longitudinal strain ε_B of the bonded length of the fibre, section B in Fig. 2, i.e.

$$\varepsilon_C = \varepsilon_B. \tag{3}$$

In the model, the fibres carry a load in the longitudinal direction only, i.e. only axial stresses appear in the free fibre segments, while in the bonded areas a biaxial stress state is considered. It is also approximated that the stresses are uniform at the bonds and shear stresses are not taken into account. To simplify, it is assumed that all fibre crossings are perpendicular, even though this is not the case in a real paper. Although some simplifications have been made the model should be able to capture the main features of the paper. If the load carrying area of a crossing fibre is equal to the cross-sectional area of the fibre, the stress in the free segments of a fibre will be the sum of the stresses in the fibres at the bonds,

$$\sigma_A = \sigma_B + \sigma_C, \tag{4}$$

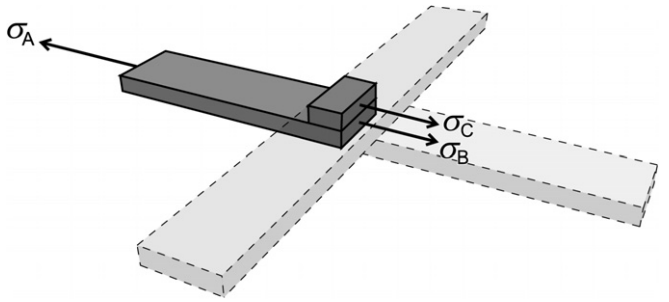

Fig. 4. Definition of the stresses σ_A, σ_B and σ_C.

where σ_A and σ_B are the stresses in the axial direction of the fibre in the free segments and at the bonds respectively, and σ_C is the transverse stress in the crossing fibre, as shown in Fig. 4.

The macroscopic specific stresses in the paper, $\bar{\sigma}^w_{11}$, $\bar{\sigma}^w_{22}$ and $\bar{\sigma}^w_{12}$, i.e. the stresses divided by the paper density, are equal to the volume average fibre stresses divided by paper density,

$$\bar{\sigma}^w_{11} = \frac{1}{\rho_f}\int_0^\pi \sigma_A f(\alpha)\cos^2\alpha\,d\alpha, \tag{5}$$

$$\bar{\sigma}^w_{22} = \frac{1}{\rho_f}\int_0^\pi \sigma_A f(\alpha)\sin^2\alpha\,d\alpha, \tag{6}$$

$$\bar{\sigma}^w_{12} = \frac{1}{\rho_f}\int_0^\pi \sigma_A f(\alpha)\cos\alpha\sin\alpha\,d\alpha, \tag{7}$$

where ρ_f is the fibre density and $f(\alpha)$ is the frequency function for the fibre angle distribution in the sheet. The frequency function must fulfil the condition

$$\int_0^\pi f(\alpha)d\alpha = 1. \tag{8}$$

Here an inhomogeneous fibre distribution is used for modelling an anisotropic paper. It is assumed that the fibres are distributed according to the frequency function

$$f(\alpha) = \frac{1}{\pi}(1 + C_1\cos 2\alpha), \tag{9}$$

where C_1 is a constant defining the degree of anisotropy in the sheet. If $C_1 = 0$ the fibres are uniformly distributed in all directions, i.e. $f(\alpha) = 1/\pi$, corresponding to an isotropic behaviour. In the previous paper (Strömbro and Gudmundson, 2008) the paper was modelled as isotropic, and therefore the frequency function was constant. As is shown later in this paper, the α-dependence of the frequency function affects some of the fibre properties, for example the fibre segment length L and therefore also λ depends on the fibre direction. These properties are also dependent on the degree of anisotropy, represented by C_1.

In the paper by Strömbro and Gudmundson (2008) a model for the constitutive relationship of a free fibre segment was derived. As an approximation, the free fibre segments between fibre-fibre bonds were modelled as two straight bars that form an angle θ, as shown in Fig. 5. Bending deformations in the bars and in the kink are approximately captured by a non-linear torsional spring. The axial displacement of the free fibre segment consists of two parts, the elongation of the bars and the displacement caused by changes in the kink angle θ. It is assumed that the normal strain of the bars can be divided into three parts, the elastic strain, the hygroexpansive strain and the creep strain. It is also assumed that the kink angle θ consist of corresponding parts, the initial angle, an elastic part, a hygroexpansive part and also a creep contribution. This fibre model captures some important features, for example an increase in moisture content will cause the curvature of an initially curved fibre to decrease. Also, the curvature of an initially curved fibre will increase with increasing compressive

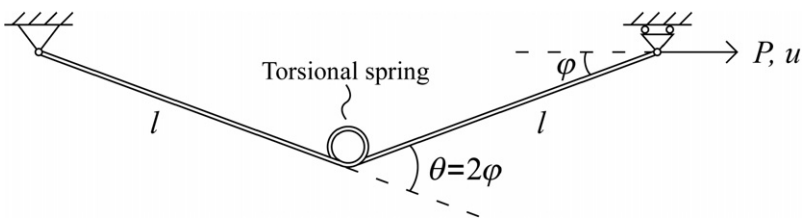

Fig. 5. The fibre model.

load and vice versa, the curvature will decrease for tensile loading. The constitutive law for the free fibre segment, section A, see Fig. 2, is given by (Strömbro and Gudmundson, 2008)

$$\varepsilon_A = \frac{\sigma_A}{E_L} + \beta_L \Delta m + \varepsilon_A^c + \frac{1}{8}(\theta_0^2 - \theta^2), \tag{10}$$

where E_L is the modulus of elasticity in the axial direction of the fibre, β_L is the hygroexpansion coefficient along the fibre and Δm is the moisture content change relative a reference level and the creep strain ε_A^c is given by the creep law (Strömbro and Gudmundson, 2008)

$$\dot{\varepsilon}_A^c = a_L \sinh(b_L(\sigma_A - E_L^c \varepsilon_A^c)), \tag{11}$$

where a_L, b_L and E_L^c are material parameters in the longitudinal direction of the fibre. Written in a slightly different form, this kind of creep law has been used to model creep of single fibres (Sedlachek, 1995). The kink angle θ is given by (Strömbro and Gudmundson, 2008)

$$\theta = \theta_0 - \frac{Al}{2k}\sigma_A \theta - (\beta_T - \beta_L)(\theta_0 + \theta_c)\Delta m + \theta_c, \tag{12}$$

$$\dot{\theta}_c = -K_1 \sinh\left(K_2\left(\frac{Al}{2}\sigma_A \theta + K_3 \theta_c\right)\right), \tag{13}$$

where θ_0 is the initial kink angle, A is the fibre cross section area, l is the length of a bar, i.e. $L_f/2$, β_L and β_T are the hygroexpansion coefficients along and transverse to the fibre and K_1, K_2 and K_3 are material parameters. The torsional spring constant k was estimated by Strömbro and Gudmundson (2008) as

$$k = q_k \frac{E_L I}{l}, \tag{14}$$

where q_k is a non-dimensional constant and I is the moment of inertia of the fibre cross section. Strömbro and Gudmundson (2008) estimated the constants K_1, K_2, K_3 as

$$K_1 = k_1 \frac{a_L l}{H}, \tag{15}$$

$$K_2 = k_2 \frac{b_L}{BH^2}, \tag{16}$$

$$K_3 = k_3 \frac{E_L^c B H^3}{l}, \tag{17}$$

where k_1, k_2, k_3 are non-dimensional constants. It is assumed that the fibres have a rectangular cross section with the width B and the height H.

In accordance with the constitutive law for the free fibre segment, the strain in the bonded segments, sections B and C, are assumed to be the sum of elastic, hygroexpansive and creep strains. As in the free fibre segment, the elastic and hygroexpansive strains are assumed to be linear functions of stresses and moisture content, respectively. The strain in section B and C then becomes

$$\varepsilon_B = \frac{\sigma_B}{E_L} + \beta_L \Delta m + \varepsilon_B^c, \tag{18}$$

$$\varepsilon_C = \frac{\sigma_C}{E_T} + \beta_T \Delta m + \varepsilon_C^c, \tag{19}$$

where E_L and E_T are the moduli of elasticity along and transverse to the fibre, β_L and β_T are the hygroexpansion coefficients along and transverse to the fibre and Δm is the moisture content change relative a reference level. The creep strains in the sections B and C, ε_B^c and ε_C^c, are given by the creep laws (Strömbro and Gudmundson, 2008)

$$\dot{\varepsilon}_B^c = a_L \sinh(b_L(\sigma_B - E_L^c \varepsilon_B^c)), \tag{20}$$

$$\dot{\varepsilon}_C^c = a_T \sinh(b_T(\sigma_C - E_T^c \varepsilon_C^c)), \tag{21}$$

where a_L, b_L and E_L^c are material parameters in the longitudinal direction of the fibre and a_T, b_T and E_T^c are material parameters transverse to the fibre.

When the moisture content in the sheet is changed, the hygroexpansive strains at the bonds of two crossing fibres will be different, i.e. in section B and C, see Fig. 2, as the hygroexpansion coefficients along and transverse fibres are different. However, since a perfect bonding is assumed, the strains are constrained according to Eq. (3), and the mismatch in hygroexpansive strains must therefore be compensated by elastic strains and creep strains, according to Eqs. (18) and (19). Elastic strains are generated immediately in the fibre bonds, producing large stresses, which are added to the stresses produced by the external loads on the paper. This gives a stress state where the absolute values of the stresses are higher than before in some of the bonded fibre sections, and in other bonded sections the absolute values of the stresses are lower than before. As the creep laws, Eqs. (11), (20), and (21), are non-linear in stress, i.e. an increase in stress leads to an increase in creep strain rate

that is higher than proportional to the stress increase, the increase in creep rate in the bonded parts with high stresses is larger than the decrease in the bonded parts with low stresses. This will lead to an increased mean strain rate, i.e. an acceleration of creep. The stresses relax, even out, as creep takes place and gradually the creep decreases by the stress relaxation as a consequence of the non-linear creep law, thus cyclic moisture content is needed to maintain the accelerated creep over a long time.

The developed fibre-network model implicitly defines a constitutive relation between specific stresses $\bar{\sigma}_{ij}^{w}$ and strains $\bar{\varepsilon}_{ij}$ on the paper (network) level, where i and j takes the values 1 and 2 denoting coordinate directions in the plane of the paper. In order to evaluate the relation all internal stress and strain variables must be eliminated. It is not possible to solve the non-linear (algebraic-differential) equations analytically, it is therefore necessary to numerically solve the problem. In this work iterative methods in MATLAB (2007) using standard routines for solving differential equations and non-linear equations are used. A detailed explanation of the numerical process can be found in Appendix A and in Strömbro and Gudmundson (2008).

3. Experimental procedures

The paper material used in this study was produced and tested by STFI-Packforsk. A description about the material and experiments are given below and more details about the experimental procedures can be found in Strömbro and Gudmundson (2008).

3.1. Material

The raw material for producing the paper material was a flash-dried unbleached kraft pulp with a Kappa number of 35. The slushed pulp was refined to 21.1° SR (WRV 1.55). The paper was produced in the EuroFEX pilot paper machine at STFI-Packforsk, using a roll former headbox, a lip opening of 13 mm, a forming concentration of 8.2 g/l, a machine speed of 400 m/min, and a jet-wire speed difference of 20 m/min. Standard fabrics and felts were used. The wet pressing was performed in three nips; a first double-felted roll press nip with a line load of 60 kN/m followed by two single-felted shoe presses with line loads 900 kN/m and 1000 kN/m, respectively. A dryness of 44.6% was reached after the last press. The paper web was wound up after wet pressing and was dried off-line under in-plane biaxial constraint in STFI-Packforsk's one-cylinder dryer. The dried paper samples were relaxed by exposing them to a climate of 23 °C and a cyclic relative humidity (RH) ranging between 50% and 90% before material testing was performed. The produced paper had a grammage of 100 g/m^2 and a structural thickness of 0.121 mm.

3.2. Testing

The hygroexpansivity tests were performed at STFI-Packforsk using a recently developed custom made apparatus that allows for measurement of the in-plane dimensions of paper test specimens in a controlled climate environment. The test specimens were 15 mm wide and a clamping length of 100 mm was used. A test piece was placed on a horizontal test table with hydrophobic surface and was clamped between two grips. One of the grips was rigidly mounted on the test table, while the other grip was mounted on a smoth-running sled. The moisture-induced changes in length of the test piece were measured by recording the movement of the sled. The in-plane dimensions of the test specimens were measured at 23 °C and at four different ambient relative humidities in the range from 50% RH to 90% RH. The measurements were performed in MD after that the tests specimens had reached moisture equilibrium.

The tensile testing of the studied paper material was performed at STFI-Packforsk in a climate room using a L&W Tensile Tester. The tensile testing was performed in both the machine direction (MD) and cross-machine direction (CD) following ISO 1924-3. Furthermore, the testing was performed for conditioned paper specimens in 23 °C and 50% RH as well as in 23 °C and 90% RH. The test pieces used were 15 mm wide and the clamping length was 100 mm. A constant strain rate of 1.67%/s was used.

The compressive tests, creep tests and mechano-sorptive creep tests were performed at STFI-Packforsk in a climate room using a custom made material testing equipment. The equipment is designed to prohibit out-of-plane buckling of thin sheet structures during in-plane loading in compression by provide lateral support of the test specimen without introducing in-plane loading (see Fig. 6). The width of the test pieces was 25 mm and the clamping length was 55 mm. The applied load was recorded by a load cell and the deformation of the test piece was measured using two LVDT's, each one connected to a surface-contacting needle that monitored displacement of the test specimen. During the compressive tests the strain rate was kept constant by using a lever and a soft spring and manually controlling the strain rate, by changing the load, until ultimate failure was detected. The target strain rate of 0.2%/s was applied. The compressive testing was performed for conditioned paper specimens in 23 °C and 50% RH as well as in 23 °C and 90% RH, in both the MD and CD.

The creep tests and the mechano-sorptive creep tests were performed under various different constant load levels in tension as well as under compression. The loading was applied by the use of a lever and a dead-weight, i.e. the load was kept constant during a test. The creep tests were performed for conditioned paper specimens in 23 °C and 50% RH as well as in 23 °C and 90% RH. The creep tests and the mechano-sorptive creep tests were performed in the MD. In the mechano-sorptive creep tests the loading was applied to the test piece at 50% RH and the test piece was then subjected to three 7 h cycles be-

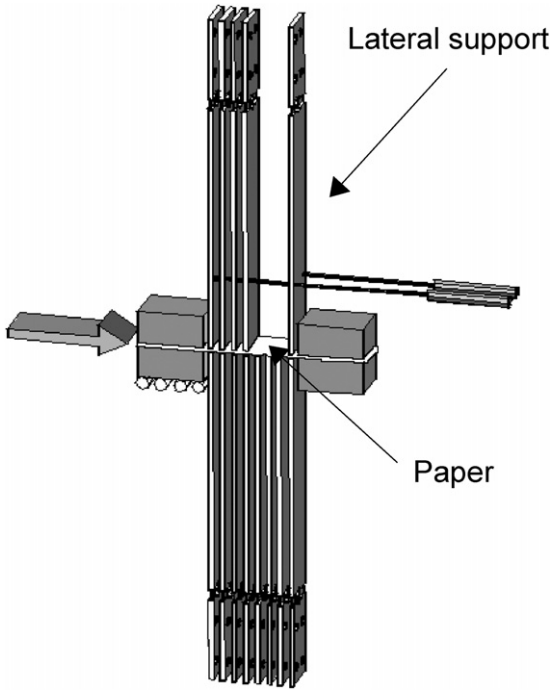

Fig. 6. An illustration of the equipment used for the compressive tests, creep tests and mechano-sorptive creep tests with lateral support of the test specimen.

tween 50% RH and 90% RH. The RH-cycle was designed so that the climate was kept constant for approximately three hours at each of the limiting relative humidities (50% and 90% RH), while the climate was ramped as rapid as possible in between these limiting relative humidities.

4. Network parameters

The number of parameters that have been introduced is quite large. They were estimated from experiments or literature data. The parameters are listed in Table 1. As the fibres should be anisotropic several material parameters are assumed to have different values along and transverse to the fibre axis. Both the elastic behaviour of the paper and the creep behaviour should be anisotropic, here this is represented by the parameters E_L, E_T, a_L, a_T, E_L^c, E_T^c. The parameters b_L and b_T are assumed to be the same since the anisotropy in the dashpot of the creep law already is included in $a_L$and a_T. It is assumed that the anisotropy, i.e. the difference in material parameters along and transverse to the fibre, can be described by a single constant $\eta > 0$, such that

$$\frac{E_L}{E_T} = \frac{E_L^c}{E_T^c} = \left(\frac{a_L}{a_T}\right)^{-1} = \eta. \tag{22}$$

This constant is assumed to be the same for creep parameters and elastic parameters. Values for the elastic ratio can be found in the literature (Schulgasser and Page, 1988; Bergander and Salmén, 2002; Salmén, 2004; Neagu, 2006).

Many of the parameters generally depend on the moisture content (Brezinski, 1956; Sedlachek, 1995). Both the elastic and creep behaviour of paper are moisture dependent. In the current creep laws it is assumed that both the springs and the dashpot have a moisture dependency. To sum up, the parameters E_L, E_T, a_L, a_T, E_L^c, E_T^c are moisture dependent. For simplicity, it is here assumed that the stiffness and creep parameters k, K_1, K_2, K_3 for the torsional springs are moisture independent. In the equations for the parameters k, K_1, K_3 for the torsional spring, see Eqs. (14), (15), and (17), parameter values for the lower moisture content m_1 was used, i.e. $E_L(m_1)$, $a_L(m_1)$, $E_L^c(m_1)$. The moisture dependent parameters are assumed to depend linearly on the moisture content according to

$$x(m) = x(m_1)\frac{m_2 - m}{m_2 - m_1} + x(m_2)\frac{m - m_1}{m_2 - m_1}, \tag{23}$$

where $x(m)$ is one of the parameters mentioned above, m is the moisture content, $x(m_1)$ and $x(m_2)$ are the values of the parameter at moisture contents m_1 and m_2 respectively. The moisture content m_1 corresponds to the low humidity used in experiments and the moisture content m_2 corresponds to the high humidity used in experiments. It is assumed that the ratio between the parameters at moisture contents m_1 and m_2 is the same for all above mentioned parameters, i.e.

Table 1
Parameters used in the network model

Parameter	Value/definition	Comment
L_{tot}	3.5 mm	Length of fibres (Niskanen, 1998)
B	35 μm	Width of the bars/fibres (Niskanen, 1998)
H	5 μm	Height of the bars/fibres (Niskanen, 1998)
ρ_f	1500 kg/m^3	Fibre density (Niskanen, 1998)
ρ_p	826 kg/m^3	Paper density, from experiments
V_f	$\rho_p/\rho_f \approx 0.55$	Volume fraction of fibres
C_1	0.7	Constant in the frequency function for the fibre distribution, see Eq. (9). Estimated from experimental stress–strain curves in CD and MD loaded in tension
θ_0^*	6.5°	Initial average kink angle, see Eq. (29). Estimated from the method described in Section 4
C_2	0.09	Constant in the distribution function for the kink angle, see Eq. (29). Estimated from the method described in Section 4
$L(\alpha)$	$\frac{L_{tot}}{n(\alpha)-1}$	Total length of fibre segment. The number of fibre bonds, $n(\alpha)$, is given by Eq. (25)
$\lambda(\alpha)$	$\frac{L_f(\alpha)}{L(\alpha)} = \frac{L(\alpha)-B}{L(\alpha)}$	Length of free fibre segment divided by total length of fibre segment
$L_f(\alpha)$	$\lambda(\alpha)L(\alpha)$	Length of free fibre segment
$l(\alpha)$	$L_f(\alpha)/2$	Length of one bar
A	$BH \approx 1.75 \cdot 10^{-10}$ m^2	Fibre cross section area, here a rectangular cross section has been assumed
I	$\frac{BH^3}{12} \approx 3.65 \cdot 10^{-22}$ m^4	Moment of inertia, here a rectangular cross section has been assumed
η	6	Anisotropy constant (Schulgasser and Page, 1988; Bergander and Salmén, 2002; Salmén, 2004; Neagu, 2006)
μ	1.3	Constant defining the moisture dependency of the parameters (Kersavage, 1973)
$m_1 = m_{ref}$	0.07	Minimum moisture content, which is equal to the starting moisture content in this study. Estimated from the experimental value 50% RH (Byrd, 1972a; Gellerstedt, 2004)
m_2	0.15	Maximum moisture content. Estimated from the experimental value 92% RH (Byrd, 1972a; Gellerstedt, 2004)
$E_L(m_1)$	37 GPa	Modulus of elasticity along the fibre at moisture level m_1, estimated from experimental stress–strain curves in tension and creep curves at $t = 0$
$E_T(m_1)$	$E_L(m_1)/\eta \approx 6.17$ GPa	Modulus of elasticity transverse to the fibre at moisture level m_1, calculated from Eq. (22)
$E_L(m_2)$	$E_L(m_1)/\mu \approx 28.5$ GPa	Modulus of elasticity along the fibre at moisture level m_2, calculated from Eq. (24)
$E_T(m_2)$	$\frac{E_L(m_2)}{\eta} = \frac{E_T(m_1)}{\mu} \approx 4.74$ GPa	Modulus of elasticity transverse to the fibre at moisture level m_1, calculated from Eq. (22) or Eq. (24)
β_L	0.013	Hygroexpansion coefficient along the fibre, estimated from experimental hygroexpansion data
β_T	$20\beta_L = 0.26$	Hygroexpansion coefficient transverse to the fibre (Niskanen, 1998)
$a_L(m_1)$	1×10^{-9} s^{-1}	Constant in the creep law along the fibre at moisture level m_1, see Eqs. (11) and (20), estimated from regular creep curves in tension
$a_T(m_1)$	$\eta a_L(m_1) = 6 \times 10^{-9}$ s^{-1}	Constant in the creep law transverse to the fibre at moisture level m_1, see Eq. (21), calculated from Eq. (22)
$a_L(m_2)$	$\mu a_L(m_1) \approx 1.3 \times 10^{-9}$ s^{-1}	Constant in the creep law along the fibre at moisture level m_2, calculated from Eq. (24)
$a_T(m_2)$	$\eta a_L(m_2) = \mu a_T(m_1)$ $\approx 7.8 \times 10^{-9}$ s^{-1}	Constant in the creep law transverse to the fibre at moisture level m_2, calculated from Eq. (22) or Eq. (24)
b_L	2×10^{-7} Pa^{-1}	Constant in the creep law along the fibre, see Eqs. (11) and (20), estimated from regular creep curves in tension
b_T	$b_L = 2 \times 10^{-7}$ Pa^{-1}	Constant in the creep law transverse to the fibre, see Eq. (21)
$E_L^c(m_1)$	2.5 GPa	Constant in the creep law along the fibre at moisture level m_1, see Eqs. (11) and (20), estimated from regular creep curves in tension
$E_T^c(m_1)$	$\frac{E_L^c(m_1)}{\eta} \approx 0.417$ GPa	Constant in the creep law transverse to the fibre at moisture level m_1, see Eq. (21), calculated from Eq. (22)
$E_L^c(m_2)$	$\frac{E_L^c(m_1)}{\mu} \approx 1.92$ GPa	Constant in the creep law along the fibre at moisture level m_2, calculated from Eq. (24)
$E_T^c(m_2)$	$\frac{E_L^c(m_2)}{\eta} = \frac{E_L^c(m_1)}{\mu} \approx 0.321$ GPa	Constant in the creep law transverse to the fibre at moisture level m_2, calculated from Eq. (22) or Eq. (24)
q_k	0.11	Constant in the equation for the torsional spring constant, Eq. (14), estimated from experimental stress–strain curve in compression and creep curves at $t = 0$
k_1	170	Constant in the creep law for the spring, see Eqs. (15) and (13), estimated from regular creep curves in compression
k_2	8	Constant in the creep law for the spring, see Eqs. (16) and (13), estimated from regular creep curves in compression
k_3	0.025	Constant in the creep law for the spring, see Eqs. (17) and (13), estimated from regular creep curves in compression
$\bar{\sigma}$	$[\sigma^w \quad 0 \quad 0]^T$ kNm/kg	Macroscopic specific stresses in the paper, for stress levels see the individual plots

$$\frac{x(m_2)}{x(m_1)} = \frac{1/E_L(m_2)}{1/E_L(m_1)} = \frac{a_L(m_2)}{a_L(m_1)} = \frac{1/E_L^c(m_2)}{1/E_L^c(m_1)} = \mu, \tag{24}$$

where μ is a constant. The same moisture dependence is found for $1/E_T$, a_T, $1/E_T^c$ according to Eq. (22).

It is assumed that the fibres in the paper are made of softwood. The length, L_{tot}, and width, B, of the fibres are chosen according to typical data for softwood (Niskanen, 1998). The number of fibre bonds can then be approximated as (Komori and Makishima, 1977)

$$n(\phi, \xi) = \frac{2V_f L_{tot}}{B} J(\phi, \xi), \tag{25}$$

where

$$J(\phi,\xi)=\int_0^{\pi}\int_0^{\pi}\Omega(\phi',\xi')\sin\chi(\phi,\xi,\phi',\xi')\sin\phi'\,\mathrm{d}\xi'\,\mathrm{d}\phi' \tag{26}$$

for a general three dimensional problem. Here a rectangular cross section has been assumed instead of the circular cross section that was used in the reference article. It is assumed that the fibre of interest has orientation (ϕ,ξ), where ϕ is the angle between the z-axis and the axis of a fibre and ξ is the angle between the x-axis and the normal projection of the fibre axis onto the xy-plane. The function $\Omega(\phi',\xi')$ is a frequency function for the fibre angle distribution that shall satisfy

$$\int_0^{\pi}\int_0^{\pi}\Omega(\phi,\xi)\sin\phi\,\mathrm{d}\xi\,\mathrm{d}\phi=1 \tag{27}$$

and χ is the angle between the fibre given by the direction (ϕ,ξ) and a fibre given by the direction (ϕ',ξ'). When all fibres are laying in the xy-plane, $\phi=\pi/2$, $\xi=\alpha$, $\sin\chi=|\sin(\alpha-a')|$, $\Omega(\phi',\xi')=f(\alpha)/2$ where $f(\alpha)$ is given by Eq. (9). This inserted into Eq. (26) gives

$$J(\alpha)=\frac{1}{\pi}\int_0^{\pi}|\sin(\alpha-\alpha')|\mathrm{d}\alpha'=\frac{2}{\pi}\left[1+\frac{C_1}{3}-\frac{2C_1}{3}\cos^2\alpha\right]. \tag{28}$$

If this value of J is used in Eq. (25), the number of fibre bonds n, and thereby also the number of fibre segments $n-1$, can be approximated. The fibre segment length L can then be estimated from the total fibre length L_{tot}, as $L=L_{\mathrm{tot}}/(n-1)$ and $\lambda=L_f/L=(L-B)/L$. It should be noted that the fibre segment length and therefore also λ depends on the fibre direction.

From experiments, by a method described in Strömbro and Gudmundson (2008), it can be estimated that there is in average one kink per fibre in a paper, and the average kink angle is approximated to be about 55°. In the paper machine, but also as a consequence of the drying conditions, the kink angle can vary between the machine direction (MD) and the cross-machine direction (CD). Because of the draw in the machine direction during manufacturing, fibres in MD are straighter than those in CD. As shown by the work of Edge (1948) the tensile stress in the machine is important. By experimental work Edge concluded that anisotropic behaviour of machine made paper under a load is not primarily a consequence of the inhomogeneous fibre distribution with more fibres in MD, but is rather due to the tensile stress in MD during manufacturing. The drying conditions are also of importance, larger kink angles are expected for freely dried paper in comparison to a paper dried under constraint. If a paper is dried under restraint in for example MD the kink angle should be larger in CD than in MD. The paper used in the present experiments was dried under restraint, with restraints in both MD and CD. The fibres become straighter under these drying conditions, but some differences in kink angles are assumed in MD compared to CD caused by the manufacturing process in the paper machine. No data about the variation of kink angle are however available from experiments, nor could it be found in the literature, but the kink angle in CD is set to be 1.5 times the kink angle in MD and the average kink angle should be 55° as described above, i.e. the kink angle in CD is 66° and MD 44°.

In the network model it is assumed that all free fibre segments have a kink, not only one kink per fibre. A suitable average kink angle per free fibre segment θ_0^* has to be found that gives a similar response as a fibre with only one large kink. The fibre model described in Section 2 was applied, but only elastic deformation was considered. The number of fibre segments is estimated by use of Eqs. (25) and (28), which gives the average number of fibre segments in fibre. The stress–strain curve for a fibre with one fibre segment with a large kink, and the other fibre segments straight, was compared to the stress–strain curve for a fibre where all free fibre segments had the same small kink angle. The kink angle in the last model, was changed until a good agreement between the two curves was found. It was not possible to get a perfect agreement for the entire interval, so special consideration to the agreement for small loads was taken, i.e. the kink angle was chosen to get the best agreement for small loads. This was done for a fibre in MD ($\alpha=0°$) and a fibre in CD ($\alpha=90°$). Then the following distribution was used,

$$\theta_0=\theta_0^*(1-C_2\cos(2\alpha)), \tag{29}$$

where the constant C_2 and the average initial kink angle θ_0^* was determined from the kink angles in MD, $\theta_0(\alpha=0°)$, and CD, $\theta_0(\alpha=90°)$, that was determined as described above. The constant C_2 and the average initial kink angle θ_0^* can be changed to model different kinds of drying conditions.

The values of the parameters in the fibre-network model were estimated from experiments or literature data, see Table 1. The parameters C_1, E_{L}, q_{k}, β_{L}, a_{L}, b_{L}, $E_{\mathrm{L}}^{\mathrm{c}}$, k_1, k_2, k_3, were fitted to experimental data. The experimental data used were provided by STFI-Packforsk and all tests were performed on the same type of kraft paper produced at STFI-Packforsk, see Section 3 for details about the material and experiments. In the mechano-sorptive creep experiments the relative humidity was varied between 50% and 92%. This corresponds approximately to moisture contents of 7% at 50% RH and 15% at 92% RH respectively (Byrd, 1972a; Gellerstedt, 2004), the data is taken from experiments on kraft paper handsheets made of southern pine pulp fibres and an unspecified paper. In the mechano-sorptive creep tests the macroscopic specific stress is prescribed along the 1-axis, $\bar{\sigma}_{11}^{\mathrm{w}}=\sigma^{\mathrm{w}}$, where σ^{w} is the value used in the experiment of current interest. When all parameters have been determined and the stress and the moisture history are set, the strains can be calculated.

The modulus of elasticity along the fibre, E_{L}, affects the elastic behaviour of the paper. To find a suitable value of the modulus of elasticity along the fibre at moisture contents m_1, $E_{\mathrm{L}}(m_1)$, the model, but only with elastic terms, was fitted to data at both 50% and 90% RH in the region of 0–15 kNm/kg from the stress–strain curves in MD (see Fig. 7a). The initial response, at $t=0$, in the tensile creep curves shown in Fig. 8 were also used when determining $E_{\mathrm{L}}(m_1)$.

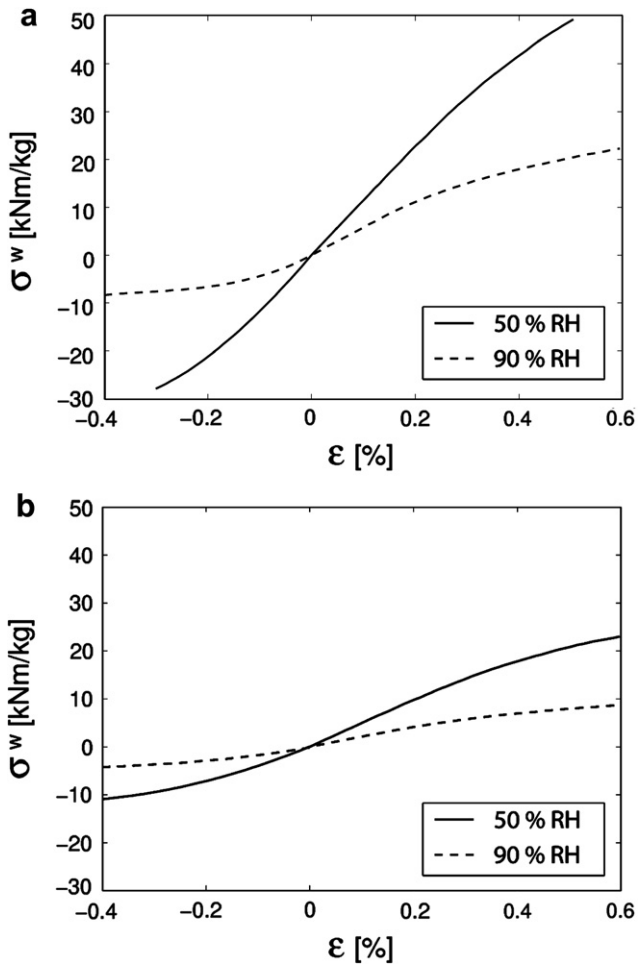

Fig. 7. Stress–strain curve composed of data from fast tension and compression tests in (a) MD and (b) CD at 50 and 90% RH, i.e. the paper should behave elastically. The curves are mean values from approximately 10 tests in tension and 10 tests in compression.

The constant q_k in the equation for the elastic torsional spring constant affects the elastic response of the kink angle, i.e. it influences mostly the elastic behaviour of the paper under compression, and can approximately be seen as the difference between the initial strain in compression and tension. To estimate q_k, data from both 50% and 90% RH stress–strain curves in MD in the region of negative stress level down to around −7 kNm/kg was used (see Fig. 7a). Only elastic terms in the model were used, i.e. no moisture variations or creep. The initial response, at $t = 0$, in the compressive creep curves shown in Fig. 9 were also used when determining q_k.

The constant C_1 in the fibre distribution frequency function affects the anisotropy in the paper and can be seen as the difference in MD and CD results, for example in the stress–strain curves shown in Fig. 7. To estimate C_1 the model, but only with elastic terms, was fitted to data from the stress–strain curves in CD, shown in Fig. 7b, for positive strains up to around 0.2%.

The hygroexpansion coefficient along the fibre, β_L, affects the response of the paper when the moisture content is changed. To find a suitable value of β_L, the model, but only with hygroexpansive strains, i.e. no applied load, was fitted to the hygroexpansion data, shown in Fig. 10. The moisture content was estimated from the relative humidity using the relationship given above.

After the constants that affect the elastic and hygroexpansive behaviour of the creep curve have been estimated, the constants affecting the creep behaviour of the paper can be approximated, starting with the constants in the creep law along the fibre, a_L, b_L, E_L^c. To find a suitable value of the creep constants at moisture contents m_1, $a_L(m_1)$, $b_L(m_1)$, $E_L^c(m_1)$, the model, with constant moisture content, was fitted to the creep curves at different tensile loads and relative humidities of 50% RH and 90% RH (see Fig. 8). As described above, a_L, E_L^c are moisture dependent, while b_L is not. This had to be taken into consideration when determining the parameters. If a change is made in $a_L(m_1)$ or $E_L^c(m_1)$, a larger effect can be seen in the creep curve at 90% RH than at 50% RH. If a_L and b_L are increased the creep is increased, while if E_L^c is increased the creep decreases. It should be noted that the time scale used in the regular creep tests (∼0–300 s) are unfortunately not the same as the one used for mechano-sorptive creep tests (∼0–70,000 s), which makes the fitting much more difficult.

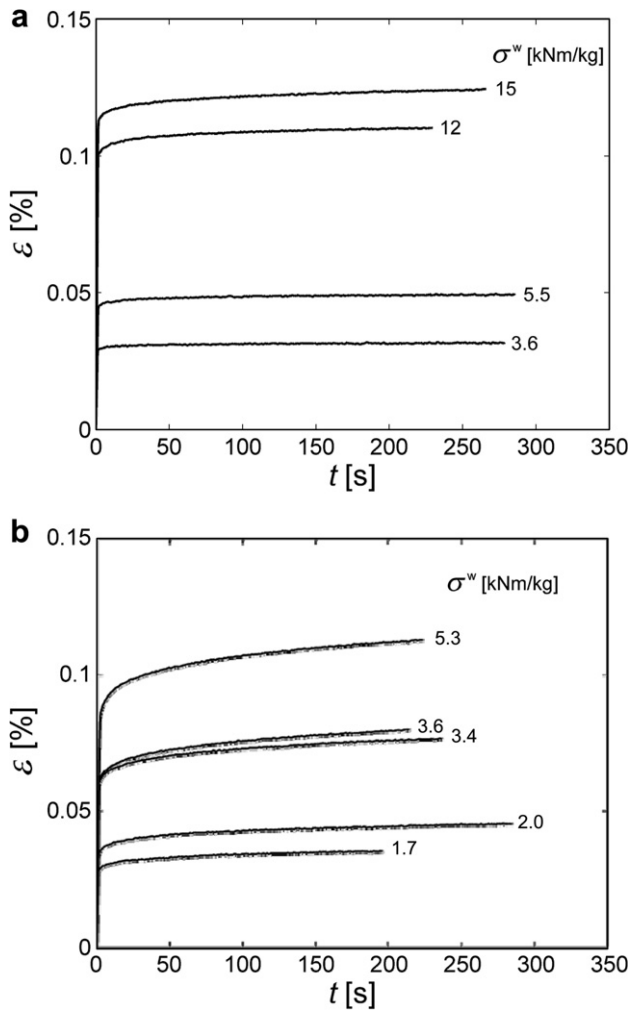

Fig. 8. Experimental creep curves with different tensile specific stresses at 50% RH (a) and 90% RH (b).

The constants k_1, k_2, k_3, that appear in the creep law for the spring, affect the creep response of the kink angle, i.e. they influence mostly the creep behaviour of the paper under compression. The model was fitted to the creep curves at different compressive loads and relative humidities of 50% RH and 90% RH (see Fig. 9). Again it should be noted that the time scale used in the regular creep tests are not the same as the one used for mechano-sorptive creep tests.

After suitable values of the constants were found the entire fitting process had to be iterated a couple of times, since changing some constants affects the results from earlier fittings, for example changing q_k changes the elastic behaviour in compression, but also gives small changes in the elastic behaviour in tension, so small changes in the modulus of elasticity had to be made.

5. Results and discussion

5.1. Comparison with experimental results

In Fig. 11 experimental mechano-sorptive creep curves under both tensile and compressive loading are presented. It can be observed that the paper creeps much faster in compression, which leads to more deformation at a given time and stress level. Mechano-sorptive creep curves determined from the present model are shown in Fig. 12. In Fig. 11(a) it is shown how the relative humidity was varied during the experiments, and in Fig. 12(a) it can be seen how the moisture content was varied in the model. If the results from the model are compared with the experimental results it can be seen that the model can capture the mechano-sorptive creep effect both under tension and compression, as well as the differences between these two load cases. As mentioned earlier, the network model presented here is a further development of the model described in an earlier work (Strömbro and Gudmundson, 2008). Mainly, moisture dependent material properties and anisotropy have

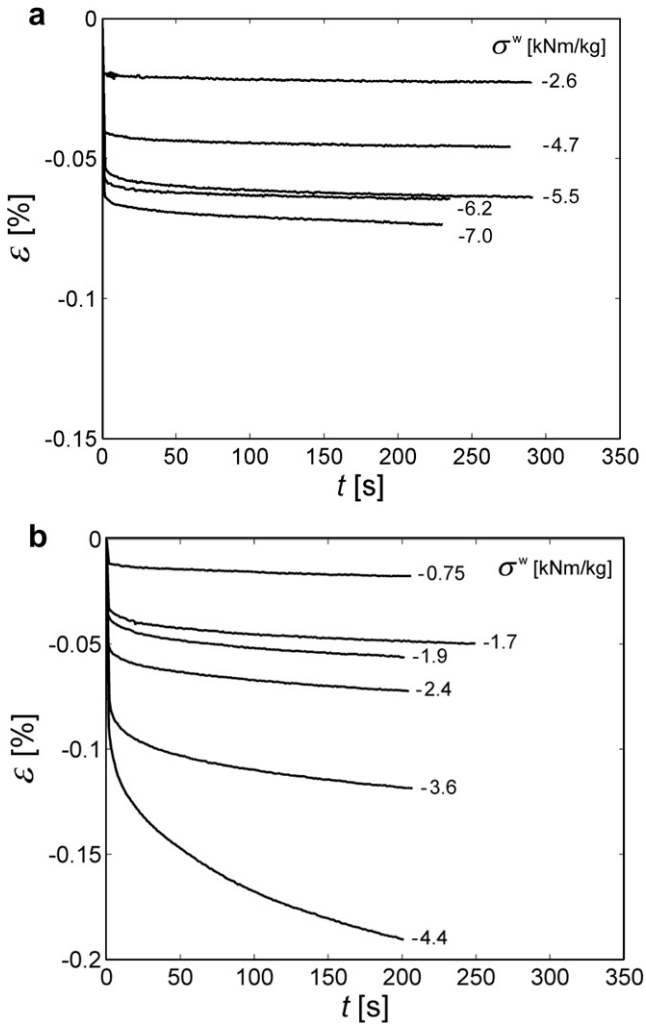

Fig. 9. Experimental creep curves with different compressive specific stresses at 50% RH (a) and 90% RH (b).

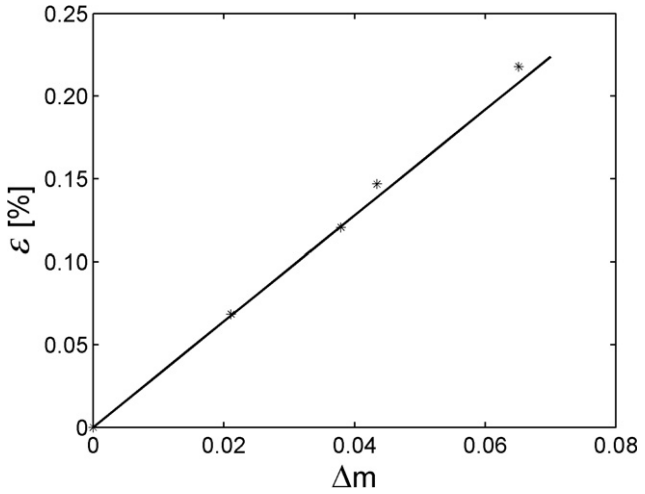

Fig. 10. Hygroexpansive strains in MD vs. relative moisture content changes. The stars represent experimentally determined strains, were each star is a mean value from around 10 test specimens. The relative humidity was varied between 50% and 84%. The line is the model fit.

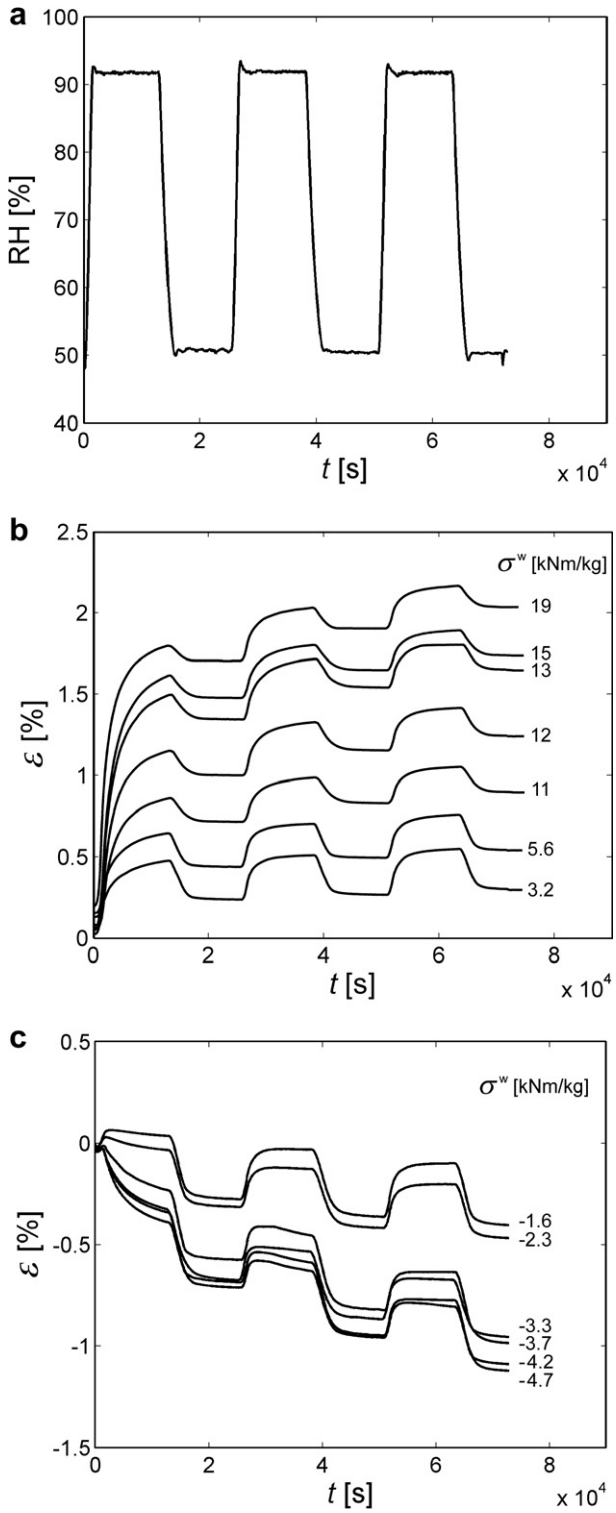

Fig. 11. Experimental mechano-sorptive creep curves where the relative humidity was varied as shown in (a). Tests were performed both with tensile (b) and compressive specific stresses applied (c).

been introduced. In Fig. 13 the results from the model presented here is compared to results from the earlier model (Strömbro and Gudmundson, 2008). It can be noted that the new development of the model has improved the results, compared to the experimental curves in Fig. 11. Especially, the mechano-sorptive creep in compression and the difference between mec-

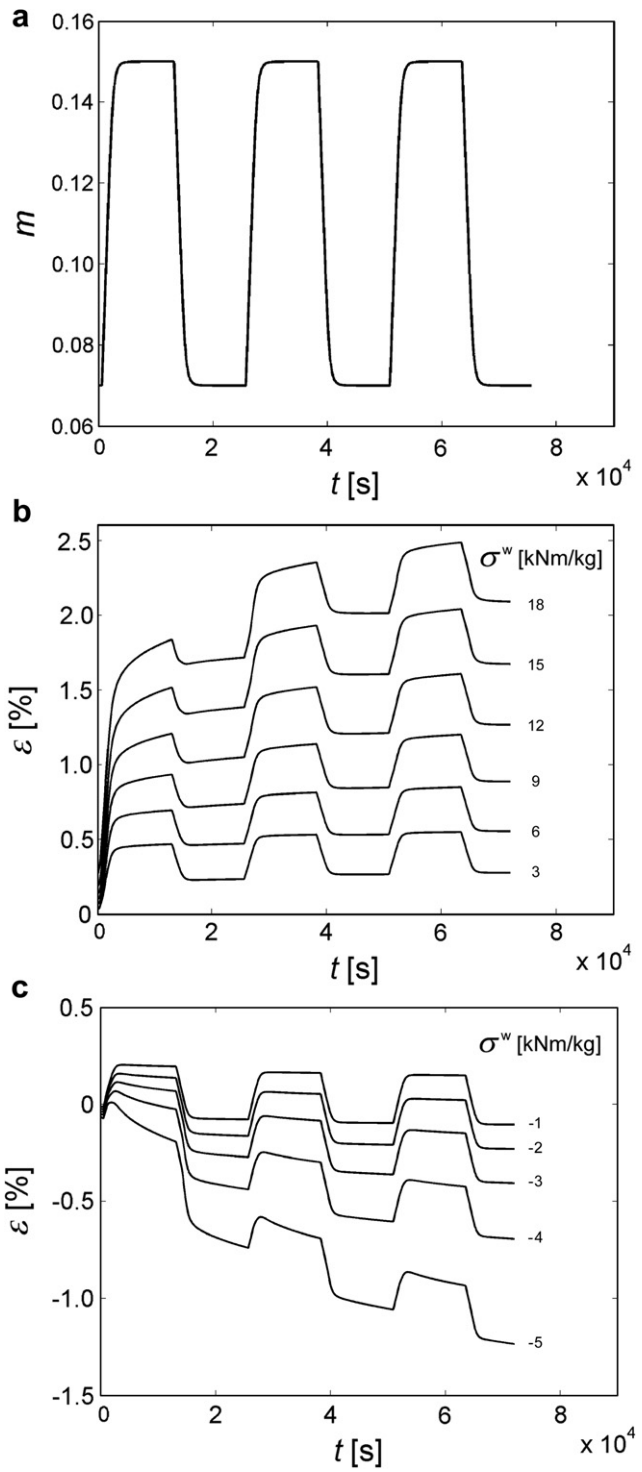

Fig. 12. Mechano-sorptive creep curves from the model where the moisture content was varied as shown in (a). Results from simulations with both tensile (b) and compressive specific stresses applied (c).

hano-sorptive creep in tension and compression is larger, which is an improvement since it agrees better with the experimental results. Another important improvement is that in the earlier model most of the creep acceleration appeared during the first moisture cycle, but now the creep is accelerated during the following cycles also. Other improvements are that the slope of the curves when the moisture is constant is larger and the different in strain between when the moisture is high and low is smaller, both changes is in agreement with the experimental results (see Figs. 11, 13, and 14).

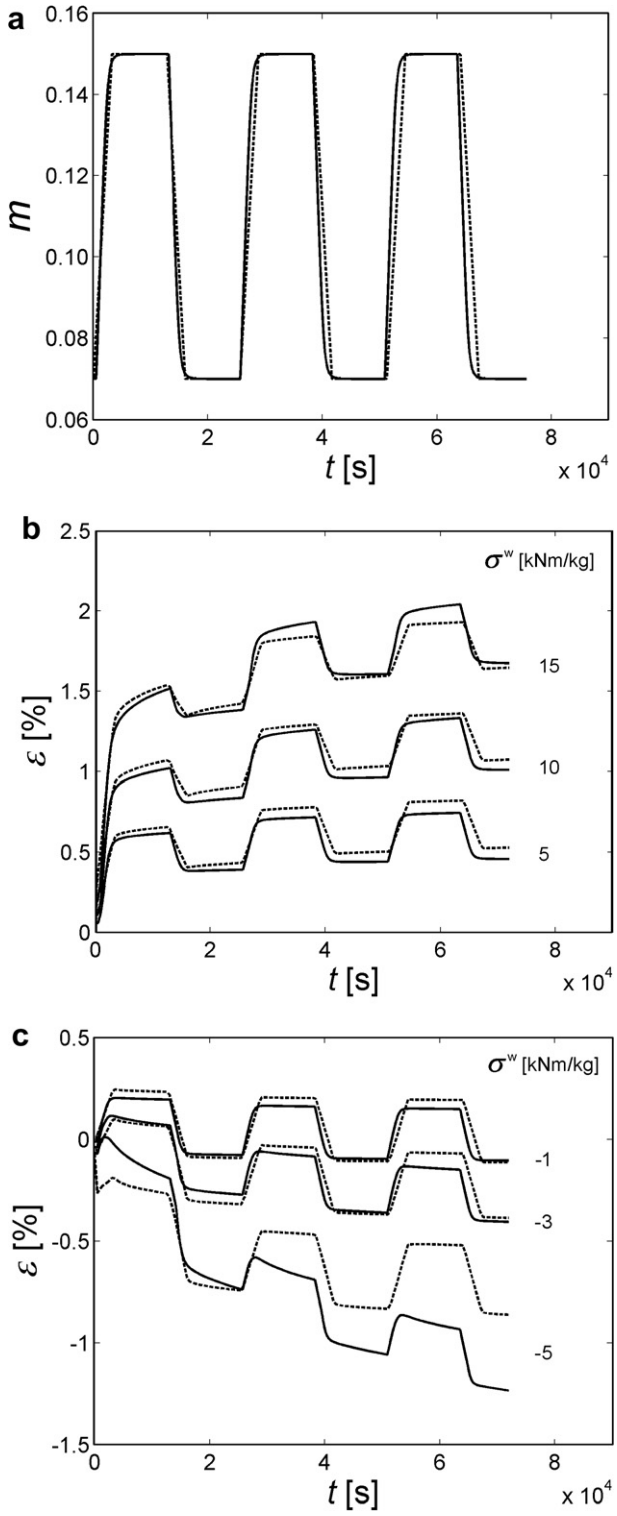

Fig. 13. Mechano-sorptive creep curves in tension (b) and compression (c) from the model presented here (—) and the model presented in Strömbro and Gudmundson (2008) (···), where the moisture content was varied as shown in (a).

By comparing the curves from the two models presented in Fig. 13(a) it can be noted that the curve that determines how the moisture content was varied in the model has been slightly changed. That is because moisture equilibrium can not be

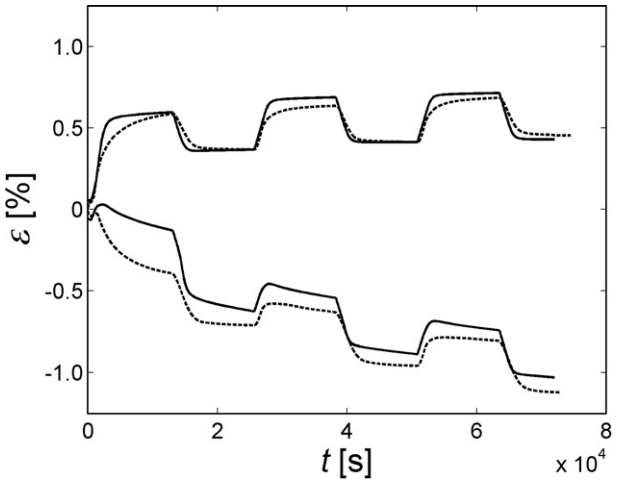

Fig. 14. Mechano-sorptive creep curves from experiments (···) and the model (—), where the same stress has been used in tension and compression, 4.7 kNm/kg.

obtained instantaneously in the paper. This change smoothens the curves somewhat but does not affect the results from the model. The shape of the mechano-sorptive curve follows the shape of the moisture curve, but the strain after each cycle is the same.

In Fig. 14 the mechano-sorptive creep curves from experiments and the model are compared for a specific stress level, both under tensile loading and compressive loading. Because the experiments under tension were not performed at the same stress levels as under compression, interpolation has been used between two curves (3.2 and 5.6 kNm/kg) to receive the curve in tension. This gives an approximate curve that is useful for comparison, although the strain is not linearly dependent on the stress. If the experimental curves and the curves from the model are compared some observations can be made. It can be noted that the predicted hygroexpansion is larger than the experimental one, at least in tension. It can also be seen that the predicted creep in compression is somewhat smaller than the experimental creep. The experimental creep curves show smoother transitions between small and large moisture contents compared to the predicted creep curves, especially in tension. This might be explained by the applied moisture content profile in Fig. 12(a) that perhaps should be even smoother. The largest difference between the experimental curves and the curves from the model can be seen in the first part of the curves, around the first moisture change. To some extent, this might be because of the applied creep law, which might not be perfect for the fibres.

To see how much the creep is accelerated by the moisture cycling, creep curves at constant high moisture content, i.e. $m = 0.15$, and mechano-sorptive creep curves are plotted in Fig. 15(b). For the mechano-sorptive creep curve the moisture was cycled according to Fig. 15(a), where the reference moisture level is $m = 0.15$, i.e. the moisture cycling begins at the high moisture level, in distinction from the moisture variation used before where the moisture reference level was the low moisture content. This enables comparisons with creep at constant moisture level. The applied load in Fig. 15(b) was 4.7 kNm/kg in tension and compression. It can be seen that the creep is accelerated both in tension and compression, but also that a larger acceleration is obtained in compression. The larger mechano-sorptive creep in compression is an effect of the extra hygroexpansion, elastic deformation and creep in compression compared to tension, that depends on the fibre model. If the fibres are modelled as straight, the paper properties become the same in compression and tension. The kinks affect the deformation under tension, but much more under compression, which leads to a more compliant behaviour in compression.

From mechano-sorptive creep curves at different stress levels, isocyclic stress–strain curves can be plotted by register the strain after a certain number of moisture cycles (here three) as a function of stress (see Fig. 16). There is a good agreement between experimental data and the isocyclic curve from the model. Both experiments and theory show a more compliant behaviour in compression compared to tension.

5.2. Drying conditions

As mentioned earlier, by changing the initial kink angle, i.e. by changing the constant C_2 and the average initial kink angle θ_0^* in Eq. (29), different kinds of drying conditions can be modelled. The parameters given in Table 1 were for a paper dried under biaxial constrains, i.e. $\theta_{0r}^* = 6.5^\circ$ and $C_{2r} = 0.09$. For a freely dried paper the fibre should have larger kink angles in all directions, so as an example θ_{0f}^* is set to be 1.5 times the initial average kink angle for the restraint paper, $\theta_{0f}^* = 1.5\theta_{0r}^*$, and the C_2 value is kept, $C_{2f} = C_{2r}$. For a paper that is restraint dried in MD and freely dried in CD, it is here assumed that the initial kink angle θ_0 is the same as the initial kink angle in the paper dried under biaxial constrains in MD and as the freely dried

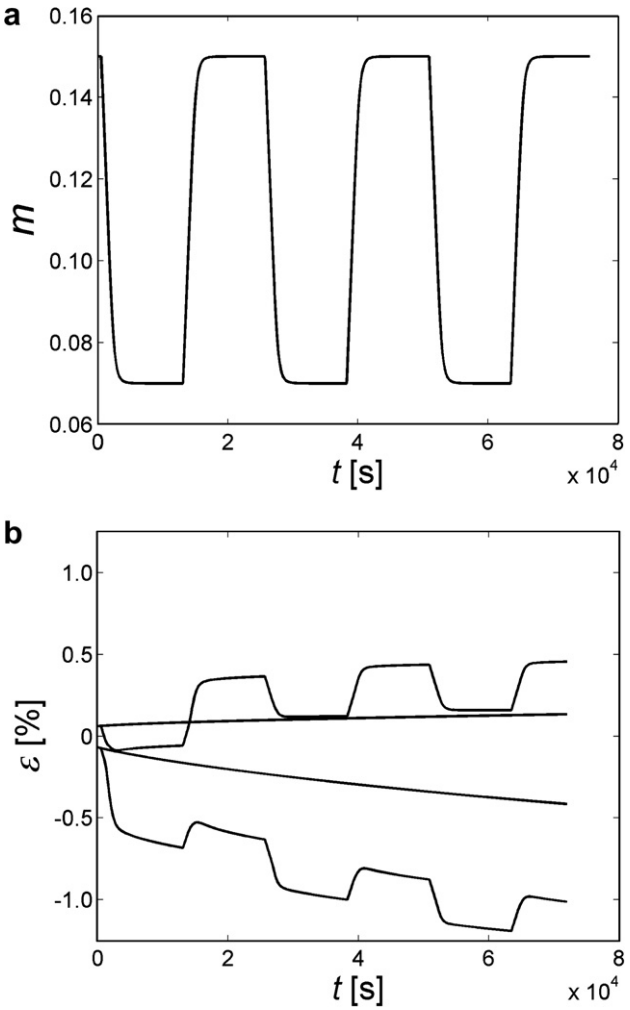

Fig. 15. Creep curves at constant high moisture content, and mechano-sorptive creep curves (b), where the moisture content was varied as shown in (a). The applied load was 4.7 kNm/kg in tension and compression.

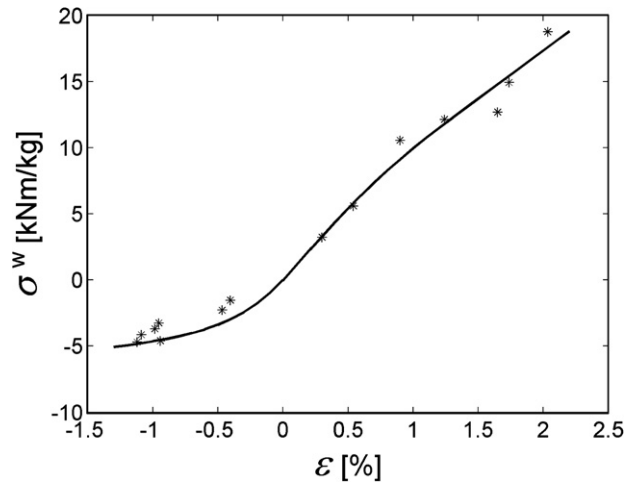

Fig. 16. Isocyclic data from experiments (∗) and from the model (—) after 3 cycles (7.2×10^4 s).

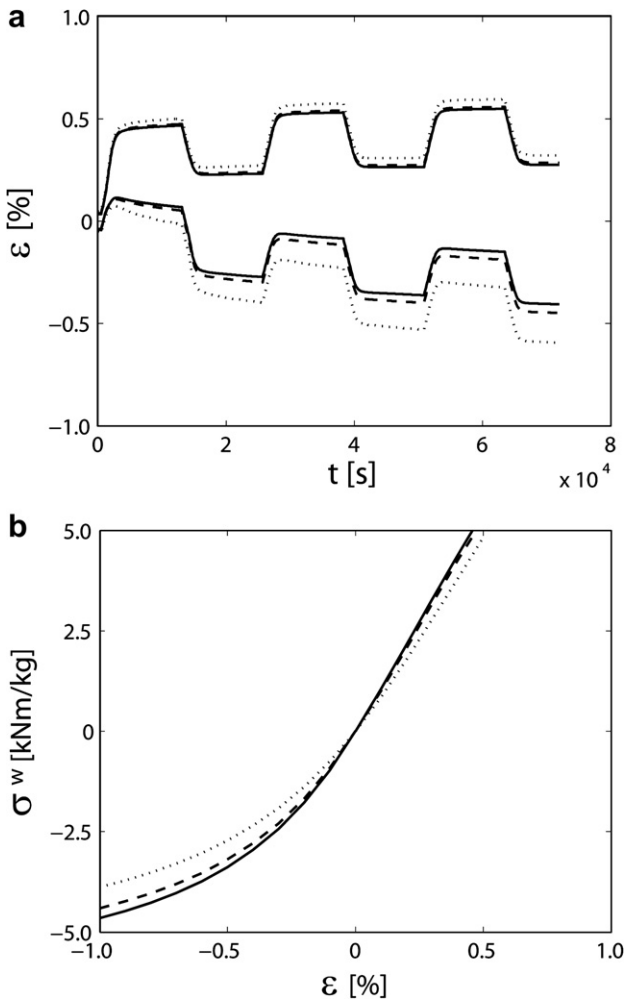

Fig. 17. Mechano-sorptive creep curves in both tension and compression where the applied load was 3 kNm/kg (a) and isocyclic curves after 3 cycles (b). The different drying conditions illustrated are, biaxial constraint (—), restraint in MD (– – –) and freely dried (···).

paper in CD. Eq. (29) gives $\theta^*_{0\mathrm{rMD}} = 1.25\theta^*_{0\mathrm{r}}$ and $C_{2\mathrm{rMD}} = 0.2$. In Fig. 17 (a) mechano-sorptive creep curves are shown and in Fig. 17 (b) isocyclic curves are shown, for the three different drying conditions in both tension and compression for this example. The paper dried freely exhibit most mechano-sorptive creep, while the paper dried under biaxial constraints exhibit the least mechano-sorptive creep, and the paper dried under restraint in MD is in between those two. The same behaviour is shown in both tension and compression. Söremark et al. (1993) found similar mechano-sorptive creep results when they experimentally compared freely dried paper with paper dried under restraint in compression. They found that a freely dried sheet had a lower compression creep stiffness index, $E^{\mathrm{w,cr}}(t) = \sigma^{\mathrm{w}}/\varepsilon(t)$, than the sheet dried under restraint. It can be noted that the curves for the paper dried under restraint in MD are closest to the curves for the paper dried under biaxial constrains so it seems that the initial fibre kink in MD is more important than the initial fibre kink in CD, at least if the load is applied in MD. In an experimental study by Fellers et al. (1999) it has been shown that straighter fibres increase the compression creep stiffness in mechano-sorptive creep, which is also in agreement with the results presented here.

6. Conclusions

In this paper a network model for mechano-sorptive creep described in an earlier work (Strömbro and Gudmundson, 2008) has been further developed. The mechano-sorptive creep effect, i.e. the creep is accelerated by moisture changes, is in the model caused by anisotropic hygroexpansion of the fibres combined with a non-linear creep law. The anisotropic hygroexpansion of the fibres produces large stresses at the fibre–fibre bonds when moisture changes. The resulting stress state will accelerate creep if the material obeys laws that are non-linear in stress. During creep the stresses created at the bonds relax, and the moisture content has to change again to maintain the accelerated creep. Fibre kinks

are included in the model in order to capture experimental observations of the differences between paper loaded in tension and compression. The further development in this paper has mainly been that moisture dependent material properties and anisotropy have been introduced. Many of the material parameters in the micromechanical model are estimated from experimental results, such as stress–strain curves, hygroexpansion curves and regular creep curves. Theoretical predictions based on the developed model are compared to experimental mechano-sorptive creep curves for an anisotropic paper both under tensile and compressive loading at varying moisture content. By introducing the anisotropy and the moisture dependent material properties the model has been improved and there are only small differences in the curves from experiments and the model. The most important experimental features are captured by the model, i.e. the creep predicted by the model is accelerated by the moisture cycling and the mechano-sorptive effect is larger in compression than in tension.

Different kinds of drying conditions have as well been examined, which showed that a freely dried paper exhibit more mechano-sorptive creep than a paper dried under restraint both in tension and compression. The model indicates that if the paper should be loaded in MD it is most important to have a restraint in the MD when the paper is dried, if low mechano-sorptive creep is desired.

The model can be improved in different ways. Certain effects like microcompressions, variations in bond angles and an improved creep law could have been considered. The uncertainty in the introduced parameters and the geometrical simplifications that are introduced in the present model would however overshadow smaller improvements in the formulation. The main features that control mechano-sorptive creep in tension and compression are included and the model is believed to be sufficiently precise to capture the main phenomena connected to mechanical loading under varying moisture conditions.

Acknowledgements

The authors are grateful to Tech. Lic. Petri Mäkelä and the Paper Mechanics cluster at STFI-Packforsk for providing experimental results.

Appendix A. Numerical solution to the network problem

Since it is not possible to solve the non-linear (differential) equations analytically, the problem is discretised and solved for a finite number of fibre angles

$$\alpha_n = \frac{(n-1)}{N}\pi, \;\; n = 1, 2, \ldots, N, \tag{A1}$$

where N is a sufficiently large number, here $N = 18$ is used. The internal variables that depend on the fibre angle α are discretised in the same way, i.e. ε_n, ε_{An}, ε_{Bn}, ε_{Cn}, ε^c_{An}, ε^c_{Bn}, ε^c_{Cn}, σ_{An}, σ_{Bn}, σ_{Cn}, θ_n, θ^c_n. Furthermore, the macroscopic strains and stresses, $\bar{\varepsilon}_{ij}$ and $\bar{\sigma}^w_{ij}$, constitute six additional variables. The network is thereby described by $12N + 6$ variables. For an anisotropic problem the fibres are not uniformly distributed, which also makes λ dependent on the fibre angle. For a general problem the initial kink angle θ_0 is also dependent on the fibre direction. The previously derived equations define, for each angle α, algebraic and differential equations for the different variables. Since many of the equations are linear, this feature can be utilized in order to eliminate certain variables. Even though many equations are linear, not all are, for example the differential equations (11), (20), and (21).

To simplify the solution, step vector notation is introduced after the discretisation. The fibre angles, which are given by Eq. (A1), can be expressed in vector notation as a $N \times 1$ vector,

$$\boldsymbol{\alpha} = \left[\, 0 \quad \tfrac{\pi}{N} \quad \tfrac{2\pi}{N} \quad \cdots \quad \tfrac{(N-1)\pi}{N} \,\right]^{\mathrm{T}}. \tag{A2}$$

The variables that depend on the fibre angle α are also expressed in vector notation, for example the average strain of the fibres can be expressed as

$$\boldsymbol{\varepsilon} = [\, \varepsilon_1 \quad \varepsilon_2 \quad \cdots \quad \varepsilon_N \,]^{\mathrm{T}}. \tag{A3}$$

In the same way can the strains and stresses in the different fibre sections, $\boldsymbol{\varepsilon_A}$, $\boldsymbol{\varepsilon_B}$, $\boldsymbol{\varepsilon_C}$, $\boldsymbol{\varepsilon^c_A}$, $\boldsymbol{\varepsilon^c_B}$, $\boldsymbol{\varepsilon^c_C}$, $\boldsymbol{\sigma_A}$, $\boldsymbol{\sigma_B}$, $\boldsymbol{\sigma_C}$, together with the kink angles $\boldsymbol{\theta}$, $\boldsymbol{\theta_0}$, $\boldsymbol{\theta_c}$, be expressed in vector notation, i.e. as $N \times 1$ vectors. The macroscopic stresses and strains are also expressed in vector notation, i.e.

$$\bar{\boldsymbol{\varepsilon}} = [\, \bar{\varepsilon}_1 \quad \bar{\varepsilon}_2 \quad \bar{\gamma}_{12} \,]^{\mathrm{T}}, \tag{A4}$$

$$\bar{\boldsymbol{\sigma}} = [\, \bar{\sigma}^w_1 \quad \bar{\sigma}^w_2 \quad \bar{\tau}^w_{12} \,]^{\mathrm{T}}. \tag{A5}$$

The equations that control the network are given by the linear Eqs. (1)–(7), (18), and (19) and the non-linear Eqs. (10) and (12). Eqs. (1), (3), (4), (18), and (19) expressed in vector notation become

$$\boldsymbol{\varepsilon} = \boldsymbol{\lambda}\boldsymbol{\varepsilon}_{\mathbf{A}} + (\mathbf{I} - \boldsymbol{\lambda})\boldsymbol{\varepsilon}_{\mathbf{B}}, \tag{A6}$$

$$\boldsymbol{\varepsilon}_{\mathbf{C}} = \boldsymbol{\varepsilon}_{\mathbf{B}}, \tag{A7}$$

$$\boldsymbol{\sigma}_{\mathbf{A}} = \boldsymbol{\sigma}_{\mathbf{B}} + \boldsymbol{\sigma}_{\mathbf{C}}, \tag{A8}$$

$$\boldsymbol{\varepsilon}_{\mathbf{B}} = \frac{\boldsymbol{\sigma}_{\mathbf{B}}}{E_{\mathrm{L}}} + \boldsymbol{\varepsilon}_{\mathbf{B}}^{\mathbf{c}} + \beta_{\mathrm{L}}\Delta m\mathbf{E}, \tag{A9}$$

$$\boldsymbol{\varepsilon}_{\mathbf{C}} = \frac{\boldsymbol{\sigma}_{\mathbf{C}}}{E_{\mathrm{T}}} + \boldsymbol{\varepsilon}_{\mathbf{C}}^{\mathbf{c}} + \beta_{\mathrm{T}}\Delta m\mathbf{E}, \tag{A10}$$

where $\mathbf{I}$ is the $N \times N$ unit matrix, $\boldsymbol{\lambda}$ is a $N \times N$ matrix with the λ values on the diagonal, i.e.

$$\boldsymbol{\lambda} = \begin{bmatrix} \lambda_1 & 0 & \cdots & 0 \\ 0 & \lambda_2 & \cdots & 0 \\ \vdots & \vdots & \ddots & 0 \\ 0 & 0 & 0 & \lambda_N \end{bmatrix} \tag{A11}$$

and $\mathbf{E}$ is a $N \times 1$ vector with ones, i.e.

$$\mathbf{E} = [\,1 \quad 1 \quad 1 \quad \cdots\,]^{\mathrm{T}}. \tag{A12}$$

The linear Eq. (2) can be expressed as

$$\boldsymbol{\varepsilon} = \boldsymbol{\Psi}\bar{\boldsymbol{\varepsilon}}, \tag{A13}$$

where $\boldsymbol{\Psi}$ is a $N \times 3$ matrix dependent on the fibre angles,

$$\boldsymbol{\Psi} = \begin{bmatrix} \cos^2\alpha_1 & \sin^2\alpha_1 & \cos\alpha_1\sin\alpha_1 \\ \cos^2\alpha_2 & \sin^2\alpha_2 & \cos\alpha_2\sin\alpha_2 \\ \vdots & \vdots & \vdots \\ \cos^2\alpha_N & \sin^2\alpha_N & \cos\alpha_N\sin\alpha_N \end{bmatrix}. \tag{A14}$$

The linear Eqs. (5)–(7) can be expressed as

$$\bar{\boldsymbol{\sigma}} = \mathbf{q}\boldsymbol{\sigma}_{\mathbf{A}}, \tag{A15}$$

where $\mathbf{q}$ is a $3 \times N$ matrix dependent on the fibre angles, the number of fibres, the fibre density and the frequency function. For the frequency function in Eq. (9), $\mathbf{q}$ reads

$$\mathbf{q} = \frac{1}{N\rho_f}\begin{bmatrix} (1 + C_1\cos 2\alpha_1)\cos^2\alpha_1 & (1 + C_1\cos 2\alpha_2)\cos^2\alpha_2 & \cdots & (1 + C_1\cos 2\alpha_N)\cos^2\alpha_N \\ (1 + C_1\cos 2\alpha_1)\sin^2\alpha_1 & (1 + C_1\cos 2\alpha_2)\sin^2\alpha_2 & \cdots & (1 + C_1\cos 2\alpha_N)\sin^2\alpha_N \\ (1 + C_1\cos 2\alpha_1)\cos\alpha_1\sin\alpha_1 & (1 + C_1\cos 2\alpha_2)\cos\alpha_2\sin\alpha_2 & \cdots & (1 + C_1\cos 2\alpha_N)\cos\alpha_N\sin\alpha_N \end{bmatrix}. \tag{A16}$$

The non-linear Eqs. (10) and (12) expressed in vector notation become

$$\boldsymbol{\varepsilon}_{\mathbf{A}} = \frac{\boldsymbol{\sigma}_{\mathbf{A}}}{E_{\mathrm{L}}} + \beta_{\mathrm{L}}\Delta m\mathbf{E} + \boldsymbol{\varepsilon}_{\mathbf{A}}^{\mathbf{c}} + \frac{1}{8}(\boldsymbol{\theta}_{\mathbf{0sq}} - \boldsymbol{\theta}_{\mathbf{sq}}), \tag{A17}$$

$$\boldsymbol{\theta} = \boldsymbol{\theta}_{\mathbf{0}} - \frac{Al^2}{2q_{\mathrm{k}}E_{\mathrm{L}}I}\mathbf{D} - (\beta_{\mathrm{T}} - \beta_{\mathrm{L}}) \cdot (\boldsymbol{\theta}_{\mathbf{0}} + \boldsymbol{\theta}_{\mathbf{c}})\Delta m + \boldsymbol{\theta}_{\mathbf{c}}, \tag{A18}$$

where Eq. (14) has been used. The vectors $\boldsymbol{\theta}_{\mathbf{0sq}}$, $\boldsymbol{\theta}_{\mathbf{sq}}$ and $\mathbf{D}$ are defined as

$$\boldsymbol{\theta}_{\mathbf{0sq}} = [\,\theta_{01}^2 \quad \theta_{02}^2 \quad \cdots \quad \theta_{0N}^2\,]^{\mathrm{T}}, \tag{A19}$$

$$\boldsymbol{\theta}_{\mathbf{sq}} = [\,\theta_1^2 \quad \theta_2^2 \quad \cdots \quad \theta_N^2\,]^{\mathrm{T}}, \tag{A20}$$

$$\mathbf{D} = [\,\sigma_{\mathrm{A}1}\theta_1 \quad \sigma_{\mathrm{A}2}\theta_2 \quad \cdots \quad \sigma_{\mathrm{A}N}\theta_N\,]^{\mathrm{T}}. \tag{A21}$$

Eqs. (A6)–(A10), (A13), (A17), and (A18), define $8N$ equations and Eq. (A15) defines three more equations. The creep laws for the kink angle and the different fibre sections, Eqs. (11), (13), (20), and (21), are valid for each fibre, for example $\dot{\varepsilon}_{\mathrm{A}1}^{\mathrm{c}} = a_{\mathrm{L}}\sinh(b_{\mathrm{L}}(\sigma_{\mathrm{A}1} - E_{\mathrm{L}}^{\mathrm{c}}\varepsilon_{\mathrm{A}1}^{\mathrm{c}}))$. This gives $4N$ additional equations. Now all equations that control the network are known. If, for example, the macroscopic specific stresses in the paper $\bar{\boldsymbol{\sigma}}$ together with the moisture variations Δm are known, then the macroscopic strains of the paper $\bar{\boldsymbol{\varepsilon}}$ and all internal variables can be determined.

If $\bar{\boldsymbol{\sigma}}$ is prescribed, Eqs. (A6)–(A10), (A13), and (A15) can be used to express $\bar{\boldsymbol{\varepsilon}}$ as

$$\bar{\boldsymbol{\varepsilon}} = \frac{1}{E_{\mathrm{L}} + E_{\mathrm{T}}}\mathbf{S}\bar{\boldsymbol{\sigma}} + \mathbf{S}\mathbf{q}(\mathbf{I} - \boldsymbol{\lambda})^{-1}\boldsymbol{\lambda}\boldsymbol{\varepsilon}_{\mathbf{A}} + \frac{E_{\mathrm{L}}}{E_{\mathrm{L}} + E_{\mathrm{T}}}\mathbf{S}\mathbf{q}(\boldsymbol{\varepsilon}_{\mathbf{B}}^{\mathbf{c}} + \beta_{\mathrm{L}}\Delta m\mathbf{E}) + \frac{E_{\mathrm{T}}}{E_{\mathrm{L}} + E_{\mathrm{T}}}\mathbf{S}\mathbf{q}(\boldsymbol{\varepsilon}_{\mathbf{C}}^{\mathbf{c}} + \beta_{\mathrm{T}}\Delta m\mathbf{E}), \tag{A22}$$

where

$$\mathbf{S} = [\mathbf{q}(\mathbf{I} - \boldsymbol{\lambda})^{-1}\boldsymbol{\Psi}]^{-1}. \tag{A23}$$

Solving Eqs. (A6)–(A10), (A13), (A15), and (A17) for the stress $\boldsymbol{\sigma}_A$ leads to the following equation,

$$\boldsymbol{\sigma}_\mathbf{A} = \mathbf{Q}\left(\mathbf{I} - \frac{1}{E_L}\mathbf{Q}\right)^{-1}\left[\frac{1}{E_L}\mathbf{R} + \boldsymbol{\varepsilon}_\mathbf{A}^\mathbf{c} + \beta_L \Delta m \mathbf{E} + \frac{1}{8}(\boldsymbol{\theta}_\mathbf{0sq} - \boldsymbol{\theta}_\mathbf{sq})\right] + \mathbf{R}, \tag{A24}$$

where

$$\mathbf{Q} = (E_L + E_T)\ (\mathbf{I} - \boldsymbol{\lambda})^{-1}(\boldsymbol{\Psi}\mathbf{S}\mathbf{q}(\mathbf{I} - \boldsymbol{\lambda})^{-1} - \mathbf{I})\ \boldsymbol{\lambda}, \tag{A25}$$

$$\mathbf{R} = (\mathbf{I} - \boldsymbol{\lambda})^{-1}\boldsymbol{\Psi}\mathbf{S}\bar{\boldsymbol{\sigma}} + [(\mathbf{I} - \boldsymbol{\lambda})^{-1}\boldsymbol{\Psi}\mathbf{S}\mathbf{q} - \mathbf{I}]\ [E_L(\boldsymbol{\varepsilon}_\mathbf{B}^\mathbf{c} + \beta_L \Delta m \mathbf{E}) + E_T(\boldsymbol{\varepsilon}_\mathbf{C}^\mathbf{c} + \beta_T \Delta m \mathbf{E})]. \tag{A26}$$

The stresses in the other parts of the fibres, $\boldsymbol{\sigma}_B$ and $\boldsymbol{\sigma}_C$, can be expressed in terms of $\boldsymbol{\sigma}_A$ by using Eqs. (A7)–(A10)

$$\boldsymbol{\sigma}_\mathbf{B} = \frac{1}{1/E_L + 1/E_T}\left[\frac{1}{E_T}\boldsymbol{\sigma}_\mathbf{A} + \boldsymbol{\varepsilon}_\mathbf{C}^\mathbf{c} - \boldsymbol{\varepsilon}_\mathbf{B}^\mathbf{c} + (\beta_T - \beta_L)\Delta m \mathbf{E}\right], \tag{A27}$$

$$\boldsymbol{\sigma}_\mathbf{C} = \frac{1}{1/E_L + 1/E_T}\left[\frac{1}{E_L}\boldsymbol{\sigma}_\mathbf{A} + \boldsymbol{\varepsilon}_\mathbf{B}^\mathbf{c} - \boldsymbol{\varepsilon}_\mathbf{C}^\mathbf{c} + (\beta_L - \beta_T)\Delta m \mathbf{E}\right]. \tag{A28}$$

To determine the macroscopic strains of the paper $\bar{\varepsilon}$, the stresses according to Eqs. (A24), (A27), and (A28) are substituted into the creep laws, Eqs. (11), (13), (20), and (21) and into the non-linear equation for the kink angle, Eq. (A18). Then Eqs. (11), (13), (20), and (21) define a system of first order ordinary differential equations that must be solved simultaneously as the non-linear equation for the kink angle, θ, Eq. (A18). The initial conditions for all creep strains and for the creep part of the kink angle is that they are zero. When the system of equations has been solved the strains $\boldsymbol{\varepsilon}_\mathbf{A}^\mathbf{c}$, $\boldsymbol{\varepsilon}_\mathbf{B}^\mathbf{c}$, $\boldsymbol{\varepsilon}_\mathbf{C}^\mathbf{c}$ and the angles θ_c, θ are known. The stresses in the different parts of the fibres, $\boldsymbol{\sigma}_A$, $\boldsymbol{\sigma}_B$ and $\boldsymbol{\sigma}_C$, can then be calculated using Eqs. (A24), (A27), and (A28). After that, the strains in the different parts of the fibres, $\boldsymbol{\varepsilon}_A$, $\boldsymbol{\varepsilon}_B$ and $\boldsymbol{\varepsilon}_C$, can be determined using Eqs. (A9), (A10), and (A17). Finally, the macroscopic strain $\bar{\varepsilon}$ can be calculated by using Eq. (A22). The introduced variables and constants K_1, K_2, K_3, $\boldsymbol{\lambda}$, $\mathbf{E}$, $\boldsymbol{\Psi}$, $\mathbf{q}$, $\boldsymbol{\theta}_\mathbf{0sq}$, $\boldsymbol{\theta}_\mathbf{sq}$, $\mathbf{D}$, $\mathbf{S}$, $\mathbf{Q}$ and $\mathbf{R}$ are given by Eqs. (15)–(17), (A11), (A12), (A14), (A16), (A19)–(A21), (A23), (A25), and (A26), respectively.

If macroscopic strains $\bar{\varepsilon}$ are prescribed instead of stresses it is possible to obtain the macroscopic stresses $\bar{\sigma}$ in a similar way as described above. The same system of equations are obtained, the only difference is $\mathbf{Q}$ and $\mathbf{R}$, which changes to

$$\mathbf{Q} = -(E_L + E_T)\ (\mathbf{I} - \boldsymbol{\lambda})^{-1}\boldsymbol{\lambda}, \tag{A29}$$

$$\mathbf{R} = (E_L + E_T)(\mathbf{I} - \boldsymbol{\lambda})^{-1}\boldsymbol{\Psi}\bar{\boldsymbol{\varepsilon}} - [E_L(\boldsymbol{\varepsilon}_\mathbf{B}^\mathbf{c} + \beta_L \Delta m \mathbf{E}) + E_T(\boldsymbol{\varepsilon}_\mathbf{C}^\mathbf{c} + \beta_T \Delta m \mathbf{E})]. \tag{A30}$$

References

Alfthan, J., Gudmundson, P., Östlund, S., 2002. A micro-mechanical model for mechano-sorptive creep in paper. Journal of Pulp and Paper Science 28 (3), 98–104.

Alfthan, J., 2003. A simplified network model for mechano-sorptive creep in paper. Journal of Pulp and Paper Science 29 (7), 228–234.

Alfthan, J., 2004. The effect of humidity cycle amplitude on accelerated tensile creep of paper. Mechanics of Time-Dependent Materials 8 (4), 289–302.

Alfthan, J., Gudmundson, P., 2005. Linear constitutive model for mechano-sorptive creep in paper. International Journal of Solids and Structures 42 (24–25), 6261–6276.

Armstrong, L.D., Kingston, R.S.T., 1960. Effect of moisture changes on creep in wood. Nature 185 (4716), 862–863.

Armstrong, L.D., Christensen, G.N., 1961. Influence of moisture changes on deformation of wood under stress. Nature 191 (4791), 869–870.

Armstrong, L.D., Kingston, R.S.T., 1962. The effect of moisture content changes on the deformation of wood under stress. Australian Journal of Applied Science 13 (4), 257–276.

Bergander, A., Salmén, L., 2002. Cell wall properties and their effects on the mechanical properties of fibers. Journal of Materials Science 37 (1), 151–156.

Brezinski, J.P., 1956. The creep properties of paper. Tappi 39 (2), 116–128.

Byrd, V.L., 1972a. Effect of relative humidity changes during creep on handsheet paper properties. Tappi 55 (2), 247–252.

Byrd, V.L., 1972b. Effect of relative humidity changes on compressive creep response of paper. Tappi 55 (11), 1612–1613.

Cox, H.L., 1952. The elasticity and strength of paper and other fibrous materials. British Journal of Applied Physics 3 (3), 72–79.

DeMaio, A., Patterson, T., 2006. Influence of bonding on the tensile creep behavior of paper in a cyclic humidity environment. Mechanics of Time-Dependent Materials 10 (1), 17–33.

DeMaio, A., Lowe, R., Patterson, T., Ragauskas, A., 2006. Direct observations of bonding influence on the tensile creep behavior of paper. Nordic Pulp and Paper Research Journal 21 (3), 297–302.

DeMaio, A., Patterson, T., 2007. Rheological modeling of the tensile creep behavior of paper. Journal of Applied Polymer Science 106 (5), 3543–3554.

DeMaio, A., Patterson, T., 2008. Similarities in bonding influence between pre-failure tensile creep and stress–strain behavior of paper. Mechanics of Materials 40 (3), 133–149.

Edge, S.R.H., 1948. Factors affecting the strength of paper. Society of Chemical Industry Journal (Chemistry and Industry) 51, 803–807.

Fellers, C., Haraldsson, T., Mohlin, U.B., 1999. Mechano-sorptive creep in compression. Influence of fibre shape and sheet structure. In: Serra-Tosio, J., Vullierme, I. (Eds.). Proceedings of the 4th International Symposium on Moisture and Creep Effects on Paper, Board and Containers, Grenoble, France, pp. 165–172.

Gallay, W., 1973. Stability of dimensions and form of paper. Tappi 56 (11), 54–63.

Gellerstedt, G. (Ed.), 2004. The Ljungberg Textbook, Paper Physics. KTH Fibre and Polymer Technology. Royal Institute of Technology (KTH), Stockholm, Sweden, p. 12 (Chapter 47).

Gibson, E.J., 1965. Creep of wood: role of water and effect of a changing moisture content. Nature 206 (4980), 213–215.

Habeger, C.C., Coffin, D.W., 2000. The role of stress concentrations in accelerated creep and sorption-induced physical aging. Journal of Pulp and Paper Science 26 (4), 145–157.
Haslach, H.W., 1994. The mechanics of moisture accelerated tensile creep in paper. Tappi Journal 77 (10), 179–186.
Hoffmeyer, P., Davidson, R.W., 1989. Mechano-sorptive creep mechanism of wood in compression and bending. Wood Science and Technology 23 (3), 215–227.
Hoffmeyer, P., 1993. Non-linear creep caused by slip plane formation. Wood Science and Technology 27 (5), 321–335.
Kersavage, P.C., 1973. Moisture content effect on tensile properties of individual Douglas-fir latewood tracheids. Wood Fiber 5 (2), 105–117.
Komori, T., Makishima, K., 1977. Numbers of fiber-to-fiber contacts in general fiber assemblies. Textile Research Journal 47 (1), 13–17.
Mackay, B.H., Downes, J.G., 1959. The effect of the sorption process on the dynamic rigidity modulus of the wool fiber. Journal of Applied Polymer Science 2 (4), 32–38.
MATLAB, 2007. MATLAB 7.4.0. The MathWorks, Inc., Natick, Massachusetts.
Mårtensson, A., 1994. Mechano-sorptive effects in wooden material. Wood Science and Technology 28 (6), 437–449.
Neagu, R.C., 2006. Hygroelastic Bahaviour of Wood-Fibre Based Materials on the Composite, Fibre and Ultrastructural Level. Ph.D. Thesis, KTH Solid Mechanics, Royal Institute of Technology (KTH), Stockholm, Sweden, pp. D20 and F9.
Niskanen, K. (Ed.), 1998. Paper Physics, Papermaking Science and Technology Book 16. Fapet Oy, Helsinki, pp. 57, 59, 91, and 233.
Nordon, P., 1962. Some torsional properties of wool fibers. Textile Research Journal 32 (7), 560–568.
Olsson, A.-M., Salmén, L., 2001. Molecular mechanisms involved in creep phenomena of paper. Journal of Applied Polymer Science 79 (9), 1590–1595.
Padanyi, Z.V., 1991. Mechano-sorptive effects and accelerated creep in paper. In: 1991 International Paper Physics Conference Proceedings, Kona, Hawaii, pp. 397–411.
Padanyi, Z.V., 1993. Physical aging and glass transition: effects on the mechanical properties of paper and board. In: Baker, C.F. (Ed.), Products of Papermaking, Transactions of the Tenth Fundamental Research Symposium Held at Oxford, vol. 1. Pira International, Leatherhead, pp. 521–545.
Pickett, G., 1942. The effect of change in moisture-content of the creep of concrete under a sustained load. Journal of the American Concrete Institute 13 (4), 333–355.
Ranta-Maunus, A., 1975. The viscoelasticity of wood at varying moisture content. Wood Science and Technology 9 (3), 189–205.
Salmén, L., 2004. Micromechanical understanding of the cell-wall structure. Comptes Rendus Biologies 327 (9–10), 873–880.
Schulgasser, K., Page, D.H., 1988. The influence of transverse fibre properties on the in-plane elastic behaviour of paper. Composites Science and Technology 32 (4), 279–292.
Sedlachek, K.M., 1995. The Effect of Hemicelluloses and Cyclic Humidity on the Creep of Single Fibers. Ph.D. Thesis, Institute of Paper Science and Technology, Atlanta, Georgia.
Strömbro, J., Gudmundson, P., 2008. Mechano-sorptive creep under compressive loading – a micromechanical model. International Journal of Solids and Structures 45 (9), 2420–2450.
Söremark, C., Fellers, C., 1993. Mechano-sorptive creep and hygroexpansion of corrugated board in bending. Journal of Pulp and Paper Science 19 (1), J19–J26.
Söremark, C., Fellers, C., Henriksson, L., 1993. Mechano-sorptive creep of paper – influence of drying restraint and fibre orientation. In: Baker, C.F. (Ed.), Products of Papermaking, Transactions of the Tenth Fundamental Research Symposium Held at Oxford, vol. 1. Pira International, Leatherhead, pp. 547–574.
Urbanik, T.J., 1995. Hygroexpansion-creep model for corrugated fiberboard. Wood and Fiber Science 27 (2), 134–140.
van den Akker, J.A., 1962. Some theoretical considerations on the mechanical properties of fibrous structures. In: Bolam, F. (Ed.), The Formation and Structure of Paper, Transactions of the Symposium Held at Oxford September 1961, vol. 1. British Paper and Board Makers Association, Technical Section, London, pp. 205–241.
Wang, J.Z., Dillard, D.A., Wolcott, M.P., Kamke, F.A., Wilkes, G.L., 1990. Transient moisture effect in fibers and composite materials. Journal of Composite Materials 24 (9), 994–1009.
Wang, J.Z., Dillard, D.A., Ward, T.C., 1992. Temperature and stress effects in the creep of aramid fibers under transient moisture conditions and discussions on the mechanism. Journal of Polymer Science Part B: Polymer Physics 30 (12), 1391–1400.
Wang, J.Z., Davé, V., Glasser, W., Dillard, D.A., 1993. The effects of moisture sorption on the creep behavior of fibers. In: Harris, C., Gates, T. (Eds.), High Temperature and Environmental Effects on Polymeric Composites, ASTM STP 1174. American Society for Testing and Materials, Philadelphia, pp. 186–200.